Journal Pre-proof

Geophysical and geochemical constraints on the origin of Holocene intraplate volcanism in East Asia

Jack F. Ward, Gideon Rosenbaum, Teresa Ubide, Jonny Wu, John T. Caulfield, Mike Sandiford, Derya Gürer

PII: S0012-8252(21)00124-0

DOI: https://doi.org/10.1016/j.earscirev.2021.103624

Reference: EARTH 103624

To appear in: *Earth-Science Reviews*

Received date: 13 October 2020

Revised date: 25 February 2021

Accepted date: 5 April 2021

Please cite this article as: J.F. Ward, G. Rosenbaum, T. Ubide, et al., Geophysical and geochemical constraints on the origin of Holocene intraplate volcanism in East Asia, *Earth-Science Reviews* (2021), https://doi.org/10.1016/j.earscirev.2021.103624

Geophysical and geochemical constraints on the origin of Holocene intraplate volcanism in East Asia

Jack F. Ward[1], Gideon Rosenbaum[1], Teresa Ubide[1], Jonny Wu[2], John T. Caulfield[1,3], Mike Sandiford[4] and Derya Gürer[1]

[1]School of Earth and Environmental Sciences, The University of Queensland, Brisbane, Queensland 4072, Australia

[2]Department of Earth and Atmospheric Sciences, University of Houston, Houston, Texas 77004, USA

[3]Central Analytical Research Facility, Queensland University of Technology, Brisbane, Queensland 4000, Australia

[4]School of Earth Sciences, University of Melbourne, Carlton, Victoria 3053, Australia

Abstract

A number of Holocene volcanoes in East Asia — Jeju, Ulleungdo, Tianchi, Longgang, Jingbohu, Erkeshan and Wudalianchi — are located far (600–1500 km) from the nearest subduction zone. The origin of these intraplate volcanoes remains unclear, and mechanisms proposed to explain their origin include plume activity and subduction processes with or without slab fluid involvement. Here we evaluate the feasibility of these mechanisms. We present an analysis of available geophysical data, including slab geometry models and the full-waveform FWEA18 tomography model, as well as statistical tests on a compilation of geochemical data. High-resolution tomography data provide no evidence for a deep-seated mantle plume. Instead, the tomography shows that Tianchi, Longgang, Jingbohu, Erkeshan and Wudalianchi are located above edges of the Pacific slab, which is stagnant near the 660 km discontinuity under East Asia. The tomography also shows that Jeju is situated

above a section of the Philippine Sea slab that has subducted to the 410 km discontinuity. While the intraplate volcanoes are underlain by subducted slabs, their geochemical signatures do not support melting via slab metasomatism typical of subduction zones. Instead, the Holocene intraplate volcanoes are alkaline and have trace element compositions comparable to those of ocean island basalts. Given the absence of geophysical or geochemical evidence for plume activity or slab metasomatism, we propose that volcanism has been generated by decompression melting associated with convective upwellings at the edges of the Pacific and Philippine Sea slabs. Tectonic reconstructions suggest that the Pacific slab may have been stagnant in the mantle transition zone for millions of years, so we speculate that localised convection at Pacific slab edges was triggered by changes in Western Pacific subduction dynamics during late Neogene–Quaternary time. The geophysical and geochemical data also suggest that Quaternary rollback of the Philippine slab might be responsible for volcanism at Jeju, which is located at the leading edge of the Philippine Sea slab.

Keywords: mantle convection; transition zone; plume; subduction-induced upwelling; mantle tomography

1. Introduction

The majority of volcanic activity on Earth is attributed to processes involving subduction zone metasomatism, lithospheric extension, or mantle plume ascent (Cañón-Tapia and Walker, 2004; Perfit and Davidson, 2000). However, some volcanoes cannot be easily explained by these three mechanisms. There are examples of volcanoes in the proximity of subduction zones that seem unrelated to mantle wedge metasomatism (Gvirtzman and Nur, 1999; Schellart, 2010; Verma, 2002), and some intraplate volcanoes show no obvious evidence of lithospheric extension or deep-seated plume activity (Christiansen et al., 2002; Finn et al., 2005). To explain the origin of such volcanism in subduction zone settings, small-scale convective processes have been invoked, involving, for

example, slab edge effects (Govers and Wortel, 2005), slab tears (Lin et al., 2004; Rosenbaum et al., 2008; Rosenbaum et al., 2018), and the interaction of slabs with the mantle transition zone (Faccenna et al., 2010). In intraplate settings, the occurrence of 'anomalous' volcanism has been ascribed to edge-driven convection associated with lithospheric steps (Demidjuk et al., 2007; King and Anderson, 1998), which can be enhanced by asthenospheric shear (Conrad et al., 2011; Davies and Rawlinson, 2014). Anomalous intraplate volcanism has also been explained by the spontaneous formation of sub-lithospheric convection below mature oceanic lithosphere (Ballmer et al., 2009) and slab-related processes operating at great distances from the trench (Faccenna et al., 2010; Mather et al., 2020; Strak and Schellart, 2014; Tang et al., 2014; Yang and Faccenda, 2020).

Subduction of the Pacific and Philippine Sea plates has been responsible for widespread Holocene arc volcanism along the margins of East Asia (Fig. 1). However, a number of Holocene volcanoes, such as Jeju, Ulleungdo, Tianchi, Longgang, Jingbohu, Erkeshan and Wudalianchi (Fig. 1), are located far (600–1500 km) from the nearest subduction zone. The origin of these volcanoes, which we herein refer to as the 'East Asian Holocene intraplate volcanoes', remains enigmatic. Previously proposed geodynamic mechanisms include the rise of deep-seated mantle plumes (Kim et al., 1998; Kimura et al., 2018; Tatsumi et al., 2004), subduction processes without slab dehydration (Brenna et al., 2015; Chen et al., 2007; Tang et al., 2014; Zou et al., 2008; Zou et al., 2003), and subduction processes involving slab dehydration (Chen et al., 2017; Zhang et al., 2018; Zhao et al., 2007).

Relationships between deep slab subduction and some of the East Asian Holocene intraplate volcanoes have been proposed on the basis of seismic tomography data and numerical models (Tang et al., 2014; Yang and Faccenda, 2020). However, a comprehensive review of relevant geophysical and geochemical data, assessing the influence of subduction-related convective processes on all of the East Asian Holocene intraplate volcanoes, has, to date, not been undertaken. The aim of this

paper is to provide such a review. The recent release of the full-waveform FWEA18 tomography model, which is one of the higher-resolution tomography models available for East Asia (Tao et al., 2018), provides an opportunity to (1) reassess previously proposed hypotheses for the origin of the East Asian Holocene intraplate volcanoes; (2) investigate the role of subduction-related convective processes in the formation of the intraplate volcanoes; and (3) develop a geodynamic model for the generation of these volcanoes. Here, we first summarise geophysical data to identify relationships between slab geometry and volcano distribution. We then perform a statistical analysis on available geochemical data to identify groupings of geochemical composition. Finally, we test the hypothesis that the spatial distribution and geochemical affinities of the East Asian Holocene intraplate volcanoes are ultimately controlled by subduction-related convective processes that induce decompression melting in the mantle.

2. Geological Setting

Quaternary arc volcanism in East Asia has occurred in response to the subduction of the Pacific and Philippine Sea plates (Fig. 1; Uto and Tatsumi, 1996). The Pacific plate subducts beneath the Eurasian and Philippine Sea plates, producing arc volcanism in the Japan–Kurile and Izu-Bonin arcs, respectively (Fig. 1; Liu et al., 2017; Sato and Amano, 1991). At the Japan Trench, the age of the subducting Pacific plate is Early Cretaceous (~130 Ma; Liu et al., 2017; Müller et al., 2008; Seton et al., 2012). The westernmost edge of the Pacific slab, which is located in the mantle transition zone below eastern China, is of Late Cretaceous age (~90 Ma; Liu et al., 2017). During most of the Cenozoic, subduction of the Pacific slab was accompanied by slab rollback, causing widespread overriding-plate extension in East Asia (Schellart and Lister, 2005). Slab rollback ended during the Miocene and since the Pliocene (~3.5 Ma), the overriding plate (at the latitude of Japan) was subjected to contractional deformation (Okada and Ikeda, 2012; Sato and Amano, 1991). The present-day plate kinematics, which involve trench advance along the Japan–Kuril and Izu-Bonin-

Marianas trenches (Faccenna et al., 2018; Heuret and Lallemand, 2005), are responsible for E–W compression in mainland East Asia (Sato and Amano, 1991; Xu, 2001; Yu et al., 2016).

The Philippine Sea plate subducts beneath the Eurasian plate in the Nankai Trough and Ryukyu Trench (Fig. 1; Faccenna et al., 2018; Nakajima and Hasegawa, 2007). Eastward retreat of the Ryukyu Trench has been responsible for back-arc extension in the Okinawa Trough (Fig. 1; Faccenna et al., 2018; Sibuet et al., 1998). The Philippine Sea plate is made up of numerous Paleogene to present back-arc basins, including the West Philippine and Shikoku-Parece Vela basins (Fig. 1; Chamot-Rooke et al., 1987; Hall, 2002; Hickey-Vargas, 2005; Hilde and Chao-Shing, 1984; Jolivet et al., 2018; Lallemand, 2016; Okino et al., 1998). The Philippine Sea plate also contains arc fragments, including the Cretaceous Amami Plateau, Oki-Daito Ridge and Daito Ridge, and the Eocene Kyushu-Palau Ridge (Fig. 1; Hickey-Vargas, 2005; Yamazaki et al., 2010).

The island of Jeju, the closest Holocene intraplate volcano to the subduction zone (Fig. 1), comprises an emergent part of a basaltic volcanic field (Brenna et al., 2012b). Phreatomagmatic activity at Jeju commenced at ~1.8 Ma (Brenna et al., 2012b; Sohn and Yoon, 2010; Sohn and Park, 2004; Yi et al., 1998). Holocene volcanic rocks erupted at Jeju include basalt, trachybasalt, basaltic andesite, basaltic trachyandesite, trachyandesite and trachydacite (Brenna et al., 2012b). To the northeast of Jeju, the eruption of 2.7 Ma basaltic agglomerates marks the onset of Ulleungdo volcanism, which continued until the mid-Holocene (Im et al., 2012). Ulleungdo volcanic rocks, characterised by extreme alkali enrichments, include tephriphonolite, trachyandesite, phonolite, and trachydacite (Brenna et al., 2014; Kim et al., 2008; Kim et al., 1999).

Two groups of Holocene intraplate volcanoes occur in eastern China. The first group includes the Jingbohu volcanic field, Tianchi (part of the Changbaishan volcanic field), and the Longgang

volcanic field (Fig. 1). The Jingbohu volcanic field consists of a volcanic plateau and a number of cinder cones and small exposed lava flows (Chen et al., 2007). Eruptions in the Jingbohu volcanic field occurred 5500–5200 years ago (Fan et al., 2003; Qicheng et al., 2006; Zou et al., 2008), producing basanite, hawaiite, trachybasalt, tephrite, phonotephrite, and foidite (Chen et al., 2007; Zou et al., 2008). Tianchi, the youngest volcano in the Changbaishan volcanic field, erupted 1000 years ago (Horn and Schmincke, 2000; Wei et al., 2007). A generalised model of eruptive history at Tianchi includes the eruption of early stage (~2.77–0.31 Ma), shield-forming basalt, a later phase of stratocone-building trachyte production, and a final episode of ignimbrite generation (Wang et al., 2003; Wei et al., 2007). In addition to these eruptive phases, volcanism at Tianchi has produced hawaiite, mugearite and basaltic andesite to peralkaline rhyolite (Chen et al., 2007). The Longgang volcanic field, in comparison, is made up of a series of cinder cones, maars and lava flows (Chen et al., 2007; Xu et al., 2003). Volcanism in the Longgang volcanic field, which occurred 1600–1500 years ago (Fan et al., 2002; Zou et al., 2003), gave rise to basalt, hawaiite, mugearite, and basaltic andesite (Chen et al., 2007).

The second group of Holocene intraplate volcanoes in eastern China includes those at Erkeshan and Wudalianchi (Fig. 1). Historical records suggest that Laoheishan and Huoshaoshan, two of the main cones in the Wudalianchi volcanic field, erupted at 1719–1721 AD (Feng and Whitford-Stark, 1986; Zou et al., 2003). Erkeshan is also considered to be of Holocene age (e.g., Chen et al., 2007). Phonotephrite, basaltic trachyandesite, tephriphonolite and trachyandesite make up eruptive sequences at both Erkeshan and Wudalianchi (Chen et al., 2007; Zhang et al., 2016; Zou et al., 2003), but Wudalianchi also contains olivine leucitite and leucite basanite (Chu et al., 2013). Based on field observations, it has been suggested that Keluo (75 km NNW of Wudalianchi) was also active during the Holocene (Global Volcanism Program, 2013), but there is no supporting geochronological evidence (Meng et al., 2018). Therefore, Keluo is not included in the list of

Holocene volcanoes discussed in this study. A number of other East Asian Holocene intraplate volcanoes are not considered in this study, either because of the paucity of geochemical data (Ch'uga-ryong; Fig.1), or because their origin has been intimately linked to plume activity (Hainan volcanic field, Udokan, Jom-Bolok, Khanui and Tariat; Xia et al., 2016; Yarmolyuk et al., 2020; Yarmolyuk et al., 2015; Zou and Fan, 2010).

3. Geophysical evaluation of the slab structure in East Asia

3.1 Approach

We utilised five geophysical datasets to evaluate the current geometry of subducted slabs and to identify potential links between slab geometry and intraplate volcanism in East Asia. The first dataset is the ISC-EHB Bulletin (Weston et al., 2018), which contains relocated earthquake hypocentres and phase arrival times from the International Seismological Centre database. The second dataset is the Global Centroid-Moment Tensor (CMT) catalogue (Dziewonski et al., 1981; Ekström et al., 2012), which comprises moment tensor data for earthquakes that occurred after 1976. The third geophysical data source is the global Slab2 model (Hayes, 2018; Hayes et al., 2018), which utilises a probabilistic non-linear fit to compute slab geometry models from a data catalogue that includes receiver function, active-source seismic interpretation, seismic tomography, and local and regional seismic data. The fourth data source contains digital mid-slab maps of the Pacific and Philippine Sea slabs (Wu et al., 2016), which were created using GOCAD software from the interpretation of the MITP08 P-wave tomography data (Li et al., 2008) and the USGS Centennial earthquake catalogue seismic data (Engdahl, 2002). The mid-slab maps include stagnant, aseismic parts of the slabs, which can be reconciled with plate reconstructions (Wu et al., 2016). Thus, relative to the Slab2 model, the mid-slab maps provide a more complete structure of the Pacific and Philippine Sea slabs. The fifth dataset is the FWEA18 tomography model (Tao et al., 2018), which is a full-waveform inversion of P- and S-wave mantle velocities from 95 magnitude 5.3–6.9

earthquakes that occurred between 2009 and 2016. Based on calculations of the preconditioned Hessian-vector product, the resolution length of the FWEA18 model in the upper mantle and transition zone below eastern China is estimated to be between 50 and 80 km, but is spatially variable depending on source–receiver configurations (Tao et al., 2018). The overall geometry of the Pacific and Philippine Sea slabs shown by the FWEA18 tomography model is similar to the slab geometry shown by the MITP08 (Li et al., 2008) and UU-P07 global tomography models (Amaru, 2007; Hall and Spakman, 2015; van der Meer et al., 2018; Supplementary Figures 1 and 2, respectively), as well as regional models of seismic tomography (Chen et al., 2017; Liu et al., 2017; Tang et al., 2014; Wei et al., 2012). To visualise the slab map and tomography data, we used *Scientific Colour Maps* (Crameri, 2018a, b).

3.2 ISC-EHB Bulletin, CMT and Slab2 data

ISC-EHB Bulletin data show abundant shallow and intermediate seismicity along the length of the Pacific slab shown by the Slab2 model (Fig. 2A). Deep seismicity (>400 km) is more sporadic, but two notable clusters of deep earthquakes occur in association with the dipping part of the Pacific slab. The largest cluster occurs east of Tianchi and Jingbohu, between 129°E and 135°E and 40°N and 45°N (Fig. 2A). According to the Slab2 model, these earthquakes correspond to the westernmost edge of the dipping part of the Pacific slab at a depth of 560 km. P-axes of these earthquakes plunge 20–40° to the west and northwest (Fig. 2B).

A second earthquake cluster occurs east of Ulleungdo (38.48°N, 134.64°E). The P-axes of these earthquakes plunge at shallow to moderate angles to the west and southwest. Deep seismicity is absent in the area immediately under the East Asian Holocene intraplate volcanoes. According to the Slab2 model, the Pacific slab is subducting below Ulleungdo, whereas the other East Asian Holocene intraplate volcanoes are located beyond the edge of this slab (Fig. 2).

3.3 Three-dimensional slab models from seismic tomography

According to the mid-slab maps (Wu et al. 2016), the subducted Pacific slab extends at least 1700 km inland from the western Pacific subduction zones (Fig. 3). The maps show that the subduction angle of the Pacific slab is steeper in the north (north of 48°N) relative to the south (Fig. 3), as indicated also by slab seismicity (Fig. 2). A roughly similar slab geometry, extending at least 1800 km inland west of the Japan Trench, has been inferred by other authors (Liu et al., 2017). The northern part of the Philippine Sea slab, according to the mid-slab maps, extends some ~800 km to the northwest of the Ryukyu Trench, reaching the 410 km discontinuity under the East China Sea (Fig. 3). Pownall et al. (2017), using a different P-wave tomography model (Amaru, 2007), also observed deep subduction of the Philippine Sea slab northwest of the Ryukyu Trench. Jeju is located close to the leading edge of the Philippine Sea slab (Fig. 3). The other East Asian Holocene intraplate volcanoes are located above areas where the mid-slab depth is >500 km (Fig. 3).

3.4 FWEA tomography data

3.4.1 Horizontal depth slices

Horizontal depth slices of the FWEA18 S-wave model (Fig. 4) show westward subduction of the Pacific slab under East Asia, which is expressed as a curvilinear, strong positive (>2.5%) dVs anomaly. The Pacific slab dVs anomaly reaches mainland East Asia at a depth of ~500 km and broadens as it approaches the 660 km discontinuity (Fig. 4C–D). Tianchi, Jingbohu, Longgang, Erkeshan and Wudalianchi are located close to edges of the Pacific slab at a depth of 600 km (Fig. 4D). The Philippine Sea slab is also identified by a positive dVs anomaly (Fig. 4A, B), which is broadest at ~400 km (Fig. 4C). Jeju is located above the leading edge of the deeper part of the Philippine Sea slab (Fig. 4C), and Ulleungdo is also located on the edge of a positive dVs anomaly (Fig. 4A–B). The latter anomaly is weaker than the Pacific slab dVs anomaly, suggesting that it

might represent part of the younger and hotter Philippine Sea slab. An alternative full waveform tomography model has also detected Philippine Sea slab, at similar depths, north of Honshu (Simutė et al., 2016). Like the FWEA18 S-wave depth slices, FWEA18 P-wave depth slices (Fig. 5) show interaction of the Pacific and Philippine Sea slabs with the 660 and 410 km discontinuities, respectively. The FWEA18 P-wave depth slices also highlight the possible positioning of the East Asian Holocene volcanoes above slab edges, which is most clearly shown in cross-sections (Figs. 6 and 7).

3.4.2 Vertical cross-sections

Vertical cross-sections of the FWEA18 S-wave tomography data show that the Pacific slab does not significantly penetrate below the 660 km discontinuity (Fig. 6). For example, a cross-section below Wudalianchi, oriented perpendicular to the strike of the Pacific slab, reveals abundant seismicity to a depth of ~300 km and the stagnation of the Pacific slab at the 660 km discontinuity (Fig. 6A). A nearly identical slab structure is revealed by the P-wave data along the same section (Fig. 7A). Both cross-sections indicate that Wudalianchi is situated near the westernmost edge of the Pacific slab.

Cross-sections below Tianchi and Longgang show seismic activity at greater depths (~600 km) and stagnation of the Pacific slab at the 660 km discontinuity (Figs 6B and 7B). A prominent negative (i.e., slow) dVs anomaly beneath Longgang and Tianchi, in the transition zone, may represent a gap in the slab (Fig. 6B), as inferred by Tang et al. (2014). Although less prominent, this gap is also visible in the P-wave tomography (Fig. 7B). However, we note that the resolution of the S-wave data is higher than that of the P-wave data (Tao et al., 2018).

The Pacific slab structure below Ulleungdo is defined by Wadati–Benioff zone seismicity to a depth of ~400 km (Figs 6C and 7C). Both the P and S-wave datasets show that the Pacific slab is stagnated

at the 660 km discontinuity. The S-wave section also shows a positive dVs anomaly that rises from the main part of the Pacific slab below Ulleungdo (Fig. 6C). Wu et al. (2016) have suggested that detached sections of Philippine Sea slab could be located in the mantle below Ulleungdo.

Cross sections beneath Jeju show subduction of both the Pacific and Philippine Sea slabs (Figs. 6D and 7D). In these sections, the Pacific slab does not penetrate into the lower mantle, but instead appears to thicken in the transition zone. Evidence of deflection of the Pacific slab at a depth of ~410 km is supported by the flattening of slab seismicity at this depth (Fig. 6D). Seismic activity associated with the Philippine Sea slab is restricted to shallower depths. The Philippine Sea slab appears to have been subducted to the 410 km discontinuity (Figs. 6D and 7D). Cross-sections below Jeju that are oriented perpendicular to the strike of the Philippine Sea slab show that Jeju is located at the western edge of the subducting Philippine Sea slab (Figs 6E and 7E).

4. Geochemical insights into the origin of East Asian Holocene intraplate volcanoes

4.1 Approach

A compilation of published geochemical data from the East Asian Holocene intraplate volcanoes, as well as East Asian Holocene arc volcanoes (labelled “EA Arc” in Figs. 8–11), is presented in Supplementary Data File 1. After evaluating differences in alkali major element compositions (Fig. 8), we examined TiO_2 and trace element data from the intraplate volcanoes to qualitatively assess source component contributions. Firstly, we constructed primitive mantle (PM) normalised multielement diagrams for samples with SiO_2 < 57 wt. % (i.e., below the andesite threshold to avoid the chemical effects of substantial magma differentiation; Fig. 9). We then compiled bivariate plots of TiO_2 and key trace element ratios (for samples with SiO_2 < 57 wt. %; Fig. 10) and compared these values to a compilation of ocean island basalt (OIB) and volcanic arc data from the PetDB Database (www.earthchem.org/petdb). We used Nb/Y to track contributions of slab melts because high field

strength elements (HFSEs), such as Nb, can be mobilised during slab melting (Hoffer et al., 2008). Enrichment of light rare earth elements (LREEs) relative to heavy rare earth elements (HREEs), represented by La/Yb, is used to infer melting in the presence of garnet (which is stable at depths >80 km; Moyen, 2009). The ratios Ba/Th and Ba/La track dehydration fluid contribution from the slab because Ba is a fluid-mobile large ion lithophile element (LILE; Hawkesworth et al., 1997a; Sun and Stern, 2001). Th is a fluid-immobile element whose mantle enrichment is affected the addition of subducted sediments, which are rich in Th (Hawkesworth et al., 1997a). Therefore, the Th/Ce ratio provides information about the addition of sediment to melts (Hawkesworth et al., 1997a; Hawkesworth et al., 1997b). Lastly, we constructed bivariate plots of (1) Nb/Th vs. Zr/Nb and (2) Zr/Y vs. Nb/Y, because these HFSE ratios are unaffected by secondary mobilisation and can be used to identify recycled components (Condie, 2003, 2005).

To identify statistically significant groupings of trace element data (normalised to normal mid-ocean ridge basalt; NMORB) from samples with SiO_2 < 57 wt. %, we used principal component analysis (PCA; Fig. 11). PCA is a dimensionality reduction technique that simplifies a dataset with a large number of variables (i.e., a dataset with a large number of 'dimensions', in our case elemental compositions) by computing new, uncorrelated variables that are linear combinations of variables included in the original dataset (Jolliffe and Cadima, 2016; Ringnér, 2008). These new variables are termed 'principal components'. The first principal component represents the direction that accounts for the largest amount of variation, and the second principal component is the orthogonal component that shows the largest variation (Abdi and Williams, 2010; Ringnér, 2008). Here, we used PCA to reduce the dimensionality of NMORB-normalised trace element data, which are traditionally plotted in a multielement 'spider diagram'. By performing PCA on trace element data (Fig. 11), differences in broad geochemical patterns can be quantitatively assessed, thus allowing us to identify similarities and differences between the normalised trace element compositions of East Asian volcanoes. PCA is

also useful because it allows visualisation of the trace element data on a single Cartesian plane, rather than many (potentially overlapping) lines on a multielement diagram. In order to avoid potential loading complications, we only included in the PCA samples that have data for Rb, Ba, Th, U, Nb, Ta, La, Ce, Pb, Pr, Sr, Nd, Sm, Zr, Hf, Eu, Tb, Dy, Er, Y, Yb and Lu.

To obtain additional information about source contributions, we used isotopic ratios, including $^{143}Nd/^{144}Nd$, $^{208}Pb/^{204}Pb$, $^{207}Pb/^{204}Pb$, $^{206}Pb/^{204}Pb$ and $^{87}Sr/^{86}Sr$ (Fig. 12). The geochemical data were processed and visualised in R (R Core Team, 2013). Packages used include ggplot2 (Wickham, 2016) and those contained in the 'tidyverse' family (Wickham et al., 2019).

4.2 Geochemical variations in the East Asian Holocene volcanoes

Relative to the East Asian arc volcanoes, the intraplate volcanoes contain significantly higher concentrations of alkalis (Fig. 8A), which possibly arise from low degrees of partial melting of an enriched source. Although both potassic and sodic rocks occur at the East Asian Holocene intraplate volcanoes (Fig. 8B), Wudalianchi and Erkeshan are considered potassic volcanoes, and Longgang, Jingbohu, Tianchi and Jeju are considered sodic volcanoes (e.g., Choi et al., 2006; Sun et al., 2017; Wang et al., 2017).

The average PM normalised trace element patterns of mafic compositions from the East Asian intraplate volcanoes are akin to those of OIBs and significantly different from the pattern of the East Asian arc basalts (Fig. 9). Relative to the arc basalts and normalised EMORB and NMORB, intraplate volcanoes are enriched in incompatible trace elements. All of the intraplate volcanoes are enriched in LREEs relative to HREEs, and they lack the prominent negative Nb and Ta anomalies (and positive Pb and Sr anomalies) characteristic of subduction-related rocks (which are shown by the East Asian arc basalts). Erkeshan and Wudalianchi are the only intraplate volcanoes that have

prominent positive Ba anomalies. Taken together, the PM normalised multielement data provide strong evidence against the involvement of subduction-related fluids.

Bivariate diagrams of TiO_2 and trace element data (from samples with SiO_2 <57 wt. %; Fig. 10) further highlight the OIB-like chemical composition of the East Asian Holocene intraplate volcanoes. For example, at a given SiO_2 concentration, the TiO_2 concentrations of the intraplate volcanoes (median TiO_2 = 2.28 ± 0.76 wt. %; Fig. 10A) are typically higher than those of the samples included in the PetDB arc compilation. Indeed, the TiO_2 values of the intraplate volcanoes fall within the OIB field. A plot of Th (ppm) vs. the Ba/Th ratio (Fig. 10B) shows that the intraplate volcanoes generally have lower Ba/Th values than the arc rocks. Exceptions to this are Erkeshan and Wudalianchi, whose elevated Ba/Th values (up to 341) are comparable to those included in the compilation of global arc rocks. The Th (ppm) values of the East Asian intraplate volcanoes are similar to those of OIBs. La/Yb and Nb/Y values (Fig. 10C) of the intraplate volcanoes are higher than those of the arc volcanoes, and, like the other trace element ratio data, the intraplate La/Yb and Nb/Y values overlap with those included in the OIB compilation. Ulleungdo contains higher Nb/Y values than the other intraplate volcanoes, but these values are similar to some OIBs. The Th/Ce and Ba/La values of the intraplate volcanoes (Fig. 10D) are typically lower than those of the arc volcanoes. The OIB-like geochemical affinities of the East Asian Holocene intraplate volcanoes are also demonstrated by bivariate plots of Nb/Th vs. Zr/Nb (Fig. 10E) and Zr/Y vs. Nb/Y (Fig. 10F).

4.3 Statistical significance of trace element variations

The PCA data for samples with SiO_2 < 57 wt. % show that principal component one (PC1) and principal component 2 (PC2) account for 59.6% and 23.4% of the observed variance, respectively (Fig. 11A). The largest contributors to PC1 are Pr, Ce, La and Nd (Fig. 11B), whereas the largest contributors to PC2 are Er, Y, Dy, Yb and Lu (Fig. 11C). Correlations between the individual

elements and the calculated principal component (PC; Fig. 11D) are also represented by vectors (Fig. 11A), where the length of the vector is directly proportional to the strength of the correlation between the individual element and the respective PC. For PC1, positive correlations are greatest with Pr, Ce, La, Nd and Zr, whereas Lu, Yb and Er are negatively correlated. For PC2, the strongest positive correlations are with Er, Y, Dy, Yb and Lu, whereas Sr, Ba, Pb and Rb are negatively correlated. Most of the East Asian arc data plot in the upper left quadrant of the PCA plot (Fig. 11A), indicating that these rocks are enriched in heavy REE relative to the intraplate rocks. Jeju is the only intraplate volcano that has data plotting in the East Asian arc field. Erkeshan and Wudalianchi plot exclusively in the lower right quadrant, indicating higher concentrations of Sr, Ba, Pb, Rb, Pr, Ce, La and Nd (i.e., LILEs and LREE) relative to the other East Asian volcanoes.

4.4 Isotope variations

A bivariate plot of $^{87}Sr/^{86}Sr$ vs. $^{143}Nd/^{144}Nd$ (Fig. 12A) shows that most of the intraplate volcanoes occur on a mixing line between depleted (DMM/FOZO) and enriched components (EM1/LoMu). $^{143}Nd/^{144}Nd$ is lowest and $^{87}Sr/^{86}Sr$ highest at Erkeshan and Wudalianchi, whereas Jingbohu and Jeju plot at the other end of the linear trend. Bivariate plots of $^{87}Sr/^{86}Sr$ vs. $^{208}Pb/^{204}Pb$ (Fig. 12B), $^{87}Sr/^{86}Sr$ vs. $^{207}Pb/^{204}Pb$ (Fig. 12C) and $^{87}Sr/^{86}Sr$ vs. $^{206}Pb/^{204}Pb$ (Fig. 12D) suggest that the unradiogenic isotope compositions of Wudalianchi and Erkeshan are similar to those of the EM1/LoMu reservoirs (e.g., Chen et al., 2007; Sun et al., 2017; Wang et al., 2017). In Jeju and Ulleungdo, the $^{208}Pb/^{204}Pb$ values are higher than those of the other intraplate volcanoes (Fig. 12B). The $^{207}Pb/^{204}Pb$ (Fig. 12C) and $^{206}Pb/^{204}Pb$ values of Jeju (Fig. 12D) are also more radiogenic than the other intraplate volcanoes. Overall, these radiogenic Pb isotope compositions indicate the inclusion of an EM2 component in the source of Jeju (e.g., Kim et al., 2019). Although the $^{207}Pb/^{204}Pb$ composition of Ulleungdo (Fig. 12C) is more radiogenic than Erkeshan and Wudalianchi, it is comparable to Tianchi, Longgang and Jingbohu. Bivariate plots of $^{206}Pb/^{204}Pb$ vs. $^{207}Pb/^{204}Pb$

(Fig. 12E) and $^{143}Nd/^{144}Nd$ vs. $^{208}Pb/^{204}Pb$ (Fig. 12F) further highlight the less radiogenic signature of Erkeshan and Wudalianchi relative to the other intraplate volcanoes, particularly Jeju and Ulleungdo.

5. Discussion

5.1 Previously proposed melting mechanisms

Holocene volcanism in East Asia has been previously explained by plume activity (Kim et al., 1998; Kimura et al., 2018; Tatsumi et al., 2004), subduction processes involving slab dehydration (Chen et al., 2017; Zhang et al., 2018; Zhao et al., 2007), and subduction processes without slab dehydration (Brenna et al., 2015; Chen et al., 2007; Tang et al., 2014; Zou et al., 2008; Zou et al., 2003). Plume-related volcanism is typically characterised by broad topographic swells, $^{3}He/^{4}He$ values of 10–30 R_A (Graham et al., 1998), and finger-like low dVp anomalies in seismic tomography (Nolet et al., 2007) with origins potentially as deep as the core–mantle boundary (Campbell, 2007; Nelson and Grand, 2018). The range of $^{3}He/^{4}He$ values (5.5–7 R_A) in the East Asian Holocene intraplate volcanoes is more akin to MORB (Chen et al., 2007), the volcanoes do not correspond to slow seismic anomalies in the lower mantle (Chen et al., 2007; Montelli et al., 2004; Tang et al., 2014), and the volume of basalt erupted is relatively small (Chen et al., 2007; Tang et al., 2014). Therefore, a mantle plume origin for these volcanoes seems unlikely.

The East Asian Holocene intraplate volcanoes are located above subducted slabs (Figs. 3–7), but the depth of the slabs below these volcanoes (> 400 km) is considerably greater than typical depths (90–150 km) associated with subduction-related volcanism (Schmidt and Poli, 1998). In addition, the volcanic rocks do not display typical subduction-related geochemical characteristics, such as calc-alkaline major element compositions, positive anomalies of fluid-mobile LILEs, and negative

anomalies of fluid-immobile HFSEs (Elliott, 2003; McCulloch and Gamble, 1991). Instead, the intraplate volcanoes have OIB-like PM normalised trace element compositions (Fig. 9).

Trace element ratio data provide further evidence that melting associated with the intraplate volcanoes was not generated by typical subduction processes. For example, the median Th/Ce value of all intraplate samples with SiO_2 <57 wt. % is 0.07, which is OIB-like and significantly lower than the values of arc rocks that have received contributions of subducted sediments (Th/Ce up to 0.35; Hawkesworth et al., 1997a). Ba/La values of the intraplate volcanoes are also lower than Ba/La values of arc rocks produced by metasomatic processes (Fig. 10D; Sun and Stern, 2001). Although only qualitative, these observations are in line with previous studies that have suggested that sediments or fluids associated with recent subduction processes do not contribute to East Asian intraplate volcanism (Brenna et al., 2015; Chen et al., 2007; Zou et al., 2008; Zou et al., 2003). The Ba/Th values (Fig. 10B) of Jeju, Ulleungdo, Jingbohu, Tianchi and Longgang are also comparable to those of MORB and OIB (Ba/Th = 50–200; Bourdon et al., 2003). Ba/Th values of Erkeshan and Wudalianchi plot within the 'subduction' field (Ba/Th = 200–1200; Bourdon et al. 2003), but these elevated values are likely associated with the long-term storage of ancient sediments in the mantle transition zone, which were added during a phase of subduction at ca. 2.2 Ga (Wang et al., 2017). The long-term isolation in the mantle transition zone of these ancient low-μ sediments, dominated by K-hollandite (which retains K, Rb, Ba and Pb; Wang et al., 2017), may also be responsible for the presence of an EM1/LoMu-like reservoir under East Asia (Sun et al., 2014; Wang et al., 2017). Indeed, Jingbohu, Tianchi, Longgang, Erkeshan and Wudalianchi appear to be the products of mixing between a depleted endmember (subcontinental lithospheric mantle for the potassic volcanoes and asthenospheric mantle for the sodic volcanoes; Wang et al., 2017; Zhang et al., 2018 and authors therein) and the EM1/LoMu reservoir associated with the mantle transition zone (Fig. 12). Mixing of a depleted component and an EM2 component of asthenospheric origin has been

invoked to explain Jeju isotope compositions (Fig. 12; Choi et al., 2014; Choi et al., 2006), and the isotope compositions of Ulleungdo likely arise from mixing of asthenospheric DMM, EM1 and EM2 components (Choi et al., 2014; Choi et al., 2006). Therefore, the isotope compositions of the East Asian Holocene intraplate volcanoes appear to reflect mixtures of mostly asthenospheric mantle sources.

Evidence of excess ^{230}Th and other observations from geochemical data (including low ^{206}Pb/^{204}Pb values, low Sr/Th values, low U/Th values, and an absence of positive K anomalies) provide further support for the lack of recent inputs of slab fluid and sediments into the East Asian Holocene intraplate volcanoes (Brenna et al., 2015; Chen et al., 2007; Sun et al., 2017; Zou et al., 2008; Zou et al., 2003). Some authors have suggested, based on the occurrence of negative δ^{26}Mg values, that mainland East Asian intraplate volcanoes originated from mantle sources that were modified by Pacific slab melts (Li et al., 2017; Yang et al., 2012; Zhang et al., 2018). However, these δ^{26}Mg anomalies have been explained by the presence of recycled carbonate-bearing sediments and carbonated eclogite, added during ancient subduction events, in the East Asian mantle (Sun et al., 2017; Wang et al., 2017). Relationships between δ^{26}Mg, Sr–Nd–Pb isotope and trace element data demonstrate the occurrence of recycled rutile-bearing eclogite and carbonate components in the Jeju mantle source, as do they preclude significant contributions of subducted sediments (Kim et al., 2019). Delivery of enriched crustal trace element and isotope signatures, characteristic of OIBs globally, to the source of East Asian Cenozoic continental intraplate basalts has also been linked to the Mesozoic rollback of the Paleo-Pacific slab, which induced rutile dehydration at post-arc depths (Xu and Zheng, 2017; Zheng et al., 2020). Bivariate plots of Nb/Th vs. Zr/Nb and Zr/Y vs. Nb/Y (Fig. 10E–F) further support the inclusion of recycled crust in the East Asian mantle. Positive correlations between 1/Os and ^{187}Os/^{188}Os (Chu et al., 2013), together with constraints from geochemical modelling (McGee et al., 2015) and correlations of various geochemical compositions

(Brenna et al., 2012a; Kimura et al., 2018; Kuritani et al., 2011; Wang et al., 2017; Zou et al., 2003), indicate that crustal contamination has not affected the geochemical composition of most East Asian Holocene intraplate basalts. Therefore, the geochemical evidence suggests that recent slab metasomatism has not significantly contributed to the composition and formation of the East Asian Holocene intraplate volcanoes. Alternatively, based on the OIB-like, LREE-enriched compositions of the intraplate volcanoes (which have been interpreted to signal melting of deep, garnet-bearing sources; Chen et al., 2007; Chu et al., 2013; Meng et al., 2018) and the proximity of the intraplate volcanoes to deep slab edges, it is possible that convection of enriched asthenospheric mantle at slab edges has led to decompression melting and the formation of these volcanoes.

5.2 Geodynamic controls on intraplate volcanism in East Asia

Most of the East Asian Holocene intraplate volcanoes are located close to and above the deep edges of the Pacific and Philippine Sea slabs, as indicated by the different geophysical datasets analysed in our study (Figs. 3–7). Mantle flow triggered by slab–mantle interaction and/or dewatering of a stagnant slab can potentially generate melting and associated alkaline volcanism (Faccenna et al., 2010). In the case of the East Asian Holocene intraplate volcanoes, however, the geochemical data do not support dewatering or fluid metasomatism. Furthermore, the Pacific slab may have been stagnant in the transition zone below East Asia for tens of millions of years (Liu et al., 2017), meaning that the cause of convective flow along the Pacific slab margin cannot be easily reconciled with the model of Faccenna et al. (2010), which predicts maximum poloidal mantle flow when the slab approaches the 660 km discontinuity. It is also difficult to apply this model to the Philippine Sea slab because this slab has not yet reached the 660 km discontinuity (Figs. 3–7).

It appears, therefore, that the origin of intraplate volcanism in East Asia should also be considered in the context of regional-scale tectonic events, which might have triggered a change in the upper

mantle convection regime (i.e., on top of the 660 km discontinuity). The onset of volcanism at Jeju, at ~1.7 Ma, coincides with a plate kinematic change expressed by (1) Philippine Sea slab rollback (Brenna et al., 2015); (2) a shift from northerly Philippine Sea plate motion to WNW-oriented migration (Wu et al., 2016); and (3) the onset of coupling between the Pacific and Caroline plates (Wu et al., 2016). Changes in the absolute plate motion of the Pacific plate occurred at ~2.6 Ma and ~0.78 Ma, involving rotation of the Pacific plate in East Asia and faster westward plate motion (Harbert and Cox, 1989; Wessel and Kroenke, 2000), which overlapped with a period of increasing Pacific slab pull force (Faccenna et al., 2012) and the onset of compressional deformation at the latitude of Japan (Okada and Ikeda, 2012; Sato and Amano, 1991). Although it is important to consider the effects of erosion on the preservation of older volcanoes, it appears that East Asian intraplate volcanic activity became more prevalent during the late Neogene and Quaternary (Fig. 13; Chen et al., 2007; Li et al., 2017; Meng et al., 2018). Given that the Pacific slab has been in the mantle transition zone since at least 10–20 Ma (Liu et al., 2017), we speculate that changes in the western Pacific subduction dynamics triggered mantle flow reorganisation, which involved convective mantle flow at the leading slab edge of the Pacific slab, that generated intraplate volcanism via decompression melting (Fig. 14). A similar mechanism has recently been proposed to explain the origin of non-age-progressive Cenozoic intraplate volcanism in eastern Australia (Mather et al., 2020). This volcanism, according to Mather et al. (2020), was generated by decompression melting of volatile-rich mantle material in response to enhanced slab flux and the perturbation of the mantle transition zone by subducted slabs. Given that the convergent margin in East Asia has been controlled predominantly by slab motion (rather than motion of the upper plate; Heuret and Lallemand, 2005), an increase of slab flux caused by regional kinematic changes could explain the dramatic increase in eruption frequency during the Quaternary (Fig. 13).

Our proposed mechanism for the origin of intraplate volcanism in East Asia is supported by analogue models (Strak and Schellart, 2014), which demonstrated that subduction-induced poloidal flow in the mantle wedge of a retreating system is greatest when a slab tip approaches depths of 450–500 km (thus explaining Jeju volcanism in response to Philippine Sea slab rollback). These analogue models have also shown that the advance of a subducted slab over the 660 km discontinuity can generate quasi-toroidal flow around lateral slab edges, as well as poloidal flow at the leading slab edge (Strak and Schellart, 2014). If so, widespread volcanism may occur along the perimeter of the Pacific and Philippine Sea slabs, raising the question why the occurrence of the intraplate volcanoes is rather sporadic. For the case of the Philippine Sea slab, it is possible that isolated decompression melting at sub-lithospheric depths was only enabled in Jeju, because it is located above the edge of the Philippine Sea slab (Figs. 3–7) and in an area that is bounded by thick lithospheric structures that could promote edge-driven convection (Song et al., 2018). For the case of the Pacific slab, indeed, many additional (Pleistocene) intraplate volcanoes are distributed along the western slab edge (Fig. 3). These Pleistocene intraplate volcanoes have OIB-like geochemical compositions comparable to those of their Holocene counterparts, lacking evidence for the incorporation of recent subduction components (e.g., Chen et al., 2007). Because the western edge of the Pacific slab was already in the mantle transition zone during Pleistocene time (Liu et al., 2017), it is possible that the Pleistocene volcanoes were also produced by slab edge convection (and associated decompression) caused by changes of subduction dynamics.

One volcano that cannot be easily explained by our proposed model is Ulleungdo, which is located several hundred kilometres away from the Pacific slab edge (Figs. 3–7). The leading edge of the Philippine Sea slab appears to occur south of Ulleungdo (Figs. 2 and 3; Simutė et al., 2016). Fast seismic anomalies below the Sea of Japan, similar to the fast S-wave anomaly below Ulleungdo, possibly represent detached fragments of Philippine Sea slab (Wu et al., 2016; Fig. 6C), which might

have played a role in triggering volcanism with a component of slab melt metasomatism (as suggested by high Nb/Y values; Fig. 11C). However, given that the potential detached slab shown by the FWEA18 tomography data is not very well resolved, the origin of Ulleungdo remains an open question.

6. Conclusion

Geophysical data suggest that the East Asian Holocene intraplate volcanoes are mostly located above deep edges of the Pacific and Philippine Sea slabs. Although the intraplate volcanoes are located above slabs, their geochemical compositions reflect minimal recent contributions of subduction fluids or sediments. Instead, the geochemical data suggest that ancient, recycled crust and sediments are included in the source of the intraplate volcanoes. Variations in isotope composition are interpreted to reflect mixing of mostly asthenospheric mantle sources. Based on these geophysical and geochemical data, we suggest that the East Asian Holocene intraplate volcanoes formed above slab edges via convective processes, involving enriched asthenospheric mantle, that may have triggered decompression melting. We also speculate that slab-edge convection could have been triggered by regional-scale tectonism associated with changes in the kinematics of the Pacific and Philippine Sea plates.

Acknowledgements

This research was funded by ARC grant DP200101566 (GR, TU and MS) and US National Science Foundation grant EAR-1848327 (JW). The manuscript benefited from comments and suggestions by Wouter Schellart and an anonymous reviewer. Sanzhong Li and Arturo Gomez-Tuena are thanked for their expert editorial handling and feedback.

Figure Captions

Figure 1: Map showing the distribution of Holocene arc volcanoes (grey triangles) and intraplate volcanoes (red and orange triangles) and regional plate boundaries of Bird (2003) in East Asia.

Figure 2: A) Map showing depth- and magnitude-calibrated East Asian seismic data of the ISC-EHB Bulletin (coloured circles), regional plate boundaries of Bird (2003), depth contours of the Slab2 model (Hayes, 2018; Hayes et al., 2018) and the distribution of Holocene arc (grey triangles) and intraplate volcanoes (red and orange triangles). B) Map showing depth- and magnitude-calibrated data of deep (>75 km) earthquakes included in the ISC-EHB Bulletin (coloured circles), P-axes of the CMT catalogue (coloured arrows), regional plate boundaries of Bird (2003), depth contours of the Slab2 model (Hayes, 2018; Hayes et al., 2018) and the distribution of Holocene arc and intraplate volcanoes (grey and red/yellow triangles respectively). The plate movement vectors are from Liu et al. (2017).

Figure 3: Map showing the mid-slab maps of Wu et al. (2016) relative to the distribution of Holocene arc volcanoes (grey triangles), Holocene intraplate volcanoes (red and orange triangles), Pleistocene intraplate volcanoes (white triangles) and regional plate boundaries of Bird (2003) in East Asia.

Figure 4: Horizontal depth slices of the FWEA18 S-wave seismic tomography model. White circles are seismic data of Engdahl (2002) that occurred within 50 km of the depth slice depth (i.e., for the 200 km depth slice, seismic events with a depth of 200 ± 50 km are shown). White triangles represent the East Asian Holocene intraplate volcanoes. The regional plate boundaries are from Bird (2003).

Figure 5: Horizontal depth slices of the FWEA18 P-wave seismic tomography model. White circles are seismic data of Engdahl (2002) that occurred within 50 km of the depth slice depth (i.e., for the 200 km depth slice, seismic events with a depth of 200 ± 50 km are shown). White triangles represent the East Asian Holocene intraplate volcanoes. The regional plate boundaries are from Bird (2003).

Figure 6: Vertical cross-sections of the FWEA18 S-wave seismic tomography model. The locations of the cross-section lines are shown in the map in the upper right-hand corner of the map. White circles are seismic data of Engdahl (2002) that occurred within 50 km of the cross-section line. White triangles represent the East Asian Holocene intraplate volcanoes.

Figure 7: Vertical cross-sections of the FWEA18 P-wave seismic tomography model. The locations of the cross-section lines are shown in the map in the upper right-hand corner of the map. White circles are seismic data of Engdahl (2002) that occurred within 50 km of the cross-section line. White triangles represent the East Asian Holocene intraplate volcanoes.

Figure 8: Anhydrous major element whole rock compositions of the East Asian Holocene volcanoes showing (A) total alkalis vs. silica (TAS diagram) and (B) K_2O vs. Na_2O. The East Asian Holocene intraplate volcanoes are, overall, more alkaline than the arc volcanoes (Fig. 8A). Fig. 8B shows that both alkaline and sodic rocks have been erupted in East Asia. Erkeshan and Wudalianchi have only erupted potassic rocks (Fig. 8B). Ulleungdo and Tianchi have erupted a combination of potassic and sodic rocks, and the remaining East Asian volcanoes have erupted sodic rocks. Data were compiled from Basu et al., 1991; Bindeman et al., 2004; Brenna et al., 2012b; Brenna et al., 2014; Chen et al., 2007; Chu et al., 2013; Hoang et al., 2013; Kita et al., 2012; Kita et al., 2001; Miyoshi et al., 2008;

Shibata et al., 2014; Sugimoto et al., 2006; Yokoyama et al., 2006; Zhang et al., 2016; Zhang et al., 1995; Zou et al., 2008; Zou et al., 2003.

Figure 9: Average PM normalised multielement compositions of the East Asian Holocene intraplate volcanoes for samples with SiO_2 <57 wt. %. PM normalised OIB, enriched mid-ocean ridge basalt (EMORB) and NMORB compositions (Sun and McDonough, 1989), as well as representative samples of main arc basalts (Kuritani et al., 2016), are displayed for comparison. Overall, the East Asian Holocene intraplate volcanoes display OIB-like trace element characteristics.

Figure 10: Bivariate plots of major and trace element data from samples with SiO_2 <57 wt. %. Data from the East Asian Holocene volcanoes are plotted over a compilation of OIB (red) and volcanic arc (blue) geochemical data from the PetDB Database (www.earthchem.org/petdb). The bivariate plots further highlight the OIB-like geochemical compositions of the East Asian Holocene intraplate volcanoes.

Figure 11: Principal component analysis (PCA) of incompatible trace element data in samples with SiO_2 <57 wt. % normalised to NMORB values of Sun and McDonough (1989). A) Variations in the two main principal components (PC1 and PC2) separate Erkeshan and Wudalianchi volcanoes from the compositions of the main arc. Vector directions and lengths represent the strength of the correlation between the individual element and the respective principal component. B) Contribution of individual elements to PC1. C) Contribution of individual elements to PC2. D) Element correlations with PC1 (orange) and PC2 (teal).

Figure 12: Bivariate plots of key isotope data from intraplate volcanoes in East Asia. Samples of all SiO_2 concentration are shown in these plots. Jeju displays the most radiogenic isotope compositions.

Erkeshan and Wudalianchi are noteworthy for displaying very low $^{208}Pb/^{204}Pb$, $^{207}Pb/^{204}Pb$ and $^{206}Pb/^{204}Pb$ values. The remaining intraplate volcanoes usually plot between the radiogenic values of Jeju and the unradiogenic values of Erkeshan and Wudalianchi. Data sources are listed in Supplementary Table 1. Isotope reservoir values are from Chen et al. (2007) and authors therein.

Figure 13: Histogram showing the occurrence of East Asian basalts younger than 110 Ma (modified from Li et al., 2017).

Figure 14: Schematic diagram of potential subduction processes that generate Holocene intraplate volcanism in East Asia. The tomography cross-sections are from Figure 6. The slab map and tomography data show that Jeju is located at the edge of the Philippine Sea slab. Quaternary slab rollback could be creating convection and decompression below at Jeju. Ulleungdo potentially overlays a detached section of the Philippine Sea slab. Tianchi, Longgang, Jingbohu, Erkeshan and Wudalianchi are located close to the edge of the Pacific slab. The late Neogene–Quaternary plate rotation and velocity increase could be generating increased convection along the edge of the Pacific slab.

9. References

Abdi, H., and Williams, L. J., 2010, Principal component analysis: Wiley interdisciplinary reviews: computational statistics, v. 2, no. 4, p. 433-459.

Amaru, M., 2007, Global travel time tomography with 3-D reference models, Utrecht University.

Ballmer, M. v., Van Hunen, J., Ito, G., Bianco, T., and Tackley, P., 2009, Intraplate volcanism with complex age-distance patterns: A case for small-scale sublithospheric convection: Geochemistry, Geophysics, Geosystems, v. 10, no. 6.

Basu, A. R., Junwen, W., Wankang, H., Guanghong, X., and Tatsumoto, M., 1991, Major element, REE, and Pb, Nd and Sr isotopic geochemistry of Cenozoic volcanic rocks of eastern China: implications for their origin from suboceanic-type mantle reservoirs: Earth and Planetary Science Letters, v. 105, no. 1-3, p. 149-169.

Bindeman, I. N., Ponomareva, V. V., Bailey, J. C., and Valley, J. W., 2004, Volcanic arc of Kamchatka: a province with high-δ 18 O magma sources and large-scale 18 O/16 O depletion of the upper crust: Geochimica et Cosmochimica Acta, v. 68, no. 4, p. 841-865.

Bird, P., 2003, An updated digital model of plate boundaries: Geochemistry, Geophysics, Geosystems, v. 4, no. 3.

Bourdon, B., Turner, S., and Dosseto, A., 2003, Dehydration and partial melting in subduction zones: Constraints from U-series disequilibria: Journal of Geophysical Research: Solid Earth, v. 108, no. B6.

Brenna, M., Cronin, S. J., Kereszturi, G., Sohn, Y. K., Smith, I. E., and Wijbrans, J., 2015, Intraplate volcanism influenced by distal subduction tectonics at Jeju Island, Republic of Korea: Bulletin of volcanology, v. 77, no. 1, p. 7.

Brenna, M., Cronin, S. J., Smith, I. E., Maas, R., and Sohn, Y. K., 2012a, How small-volume basaltic magmatic systems develop: a case study from the Jeju Island Volcanic Field, Korea: Journal of Petrology, v. 53, no. 5, p. 985-1018.

Brenna, M., Cronin, S. J., Smith, I. E., Sohn, Y. K., and Maas, R., 2012b, Spatio-temporal evolution of a dispersed magmatic system and its implications for volcano growth, Jeju Island Volcanic Field, Korea: Lithos, v. 148, p. 337-352.

Brenna, M., Price, R., Cronin, S. J., Smith, I. E., Sohn, Y. K., Kim, G. B., and Maas, R., 2014, Final magma storage depth modulation of explosivity and trachyte–phonolite genesis at an intraplate volcano: a case study from Ulleung Island, South Korea: Journal of Petrology, v. 55, no. 4, p. 709-747.

Campbell, I. H., 2007, Testing the plume theory: Chemical Geology, v. 241, no. 3-4, p. 153-176.

Cañón-Tapia, E., and Walker, G. P., 2004, Global aspects of volcanism: the perspectives of "plate tectonics" and "volcanic systems": Earth-Science Reviews, v. 66, no. 1-2, p. 163-182.

Chamot-Rooke, N., Renard, V., and Le Pichon, X., 1987, Magnetic anomalies in the Shikoku Basin: a new interpretation: Earth and Planetary Science Letters, v. 83, no. 1-4, p. 214-228.

Chen, C., Zhao, D., Tian, Y., Wu, S., Hasegawa, A., Lei, J., Park, J.-H., and Kang, I.-B., 2017, Mantle transition zone, stagnant slab and intraplate volcanism in Northeast Asia: Geophysical Journal International, v. 209, no. 1, p. 68-85.

Chen, Y., Zhang, Y., Graham, D., Su, S., and Deng, J., 2007, Geochemistry of Cenozoic basalts and mantle xenoliths in Northeast China: Lithos, v. 96, no. 1, p. 108-126.

Choi, H.-O., Choi, S. H., and Yu, Y., 2014, Isotope geochemistry of Jeongok basalts, northernmost South Korea: implications for the enriched mantle end-member component: Journal of Asian Earth Sciences, v. 91, p. 56-68.

Choi, S. H., Mukasa, S. B., Kwon, S.-T., and Andronikov, A. V., 2006, Sr, Nd, Pb and Hf isotopic compositions of late Cenozoic alkali basalts in South Korea: Evidence for mixing between the two dominant asthenospheric mantle domains beneath East Asia: Chemical Geology, v. 232, no. 3-4, p. 134-151.

Christiansen, R. L., Foulger, G., and Evans, J. R., 2002, Upper-mantle origin of the Yellowstone hotspot: Geological Society of America Bulletin, v. 114, no. 10, p. 1245-1256.

Chu, Z.-Y., Harvey, J., Liu, C.-Z., Guo, J.-H., Wu, F.-Y., Tian, W., Zhang, Y.-L., and Yang, Y.-H., 2013, Source of highly potassic basalts in northeast China: evidence from Re–Os, Sr–Nd–Hf isotopes and PGE geochemistry: Chemical Geology, v. 357, p. 52-66.

Condie, K. C., 2003, Incompatible element ratios in oceanic basalts and komatiites: tracking deep mantle sources and continental growth rates with time: Geochemistry, Geophysics, Geosystems, v. 4, no. 1, p. 1-28.

Condie, K. C., 2005, High field strength element ratios in Archean basalts: a window to evolving sources of mantle plumes?: Lithos, v. 79, no. 3-4, p. 491-504.

Conrad, C. P., Bianco, T. A., Smith, E. I., and Wessel, P., 2011, Patterns of intraplate volcanism controlled by asthenospheric shear: Nature Geoscience, v. 4, no. 5, p. 317-321.

Crameri, F., 2018a, Geodynamic diagnostics, scientific visualisation and StagLab 3.0: Geoscientific Model Development, v. 11, no. 6, p. 2541-2562.

Crameri, F., 2018b, Scientific colour-maps: Zenodo. doi, v. 10.

Davies, D. R., and Rawlinson, N., 2014, On the origin of recent intraplate volcanism in Australia: Geology, v. 42, no. 12, p. 1031-1034.

Demidjuk, Z., Turner, S., Sandiford, M., George, R., Foden, J., and Etheridge, M., 2007, U-series isotope and geodynamic constraints on mantle melting processes beneath the Newer Volcanic Province in South Australia: Earth and Planetary Science Letters, v. 261, no. 3-4, p. 517-533.

Dziewonski, A., Chou, T. A., and Woodhouse, J., 1981, Determination of earthquake source parameters from waveform data for studies of global and regional seismicity: Journal of Geophysical Research: Solid Earth, v. 86, no. B4, p. 2825-2852.

Ekström, G., Nettles, M., and Dziewoński, A., 2012, The global CMT project 2004–2010: Centroid-moment tensors for 13,017 earthquakes: Physics of the Earth and Planetary Interiors, v. 200, p. 1-9.

Elliott, T., 2003, Tracers of the slab: GEOPHYSICAL MONOGRAPH-AMERICAN GEOPHYSICAL UNION, v. 138, p. 23-46.

Engdahl, E. R., 2002, Global seismicity: 1900-1999: International handbook of earthquake and engineering seismology, p. 665-690.

Faccenna, C., Becker, T. W., Lallemand, S., Lagabrielle, Y., Funiciello, F., and Piromallo, C., 2010, Subduction-triggered magmatic pulses: A new class of plumes?: Earth and Planetary Science Letters, v. 299, no. 1-2, p. 54-68.

Faccenna, C., Becker, T. W., Lallemand, S., and Steinberger, B., 2012, On the role of slab pull in the Cenozoic motion of the Pacific plate: Geophysical Research Letters, v. 39, no. 3.

Faccenna, C., Holt, A. F., Becker, T. W., Lallemand, S., and Royden, L. H., 2018, Dynamics of the Ryukyu/Izu-Bonin-Marianas double subduction system: Tectonophysics, v. 746, p. 229-238.

Fan, Q., Sui, J., Liu, R., Wei, H., Li, D., Sun, Q., and Li, N., 2002, Periods of Quarternary volcanic activity in Longgang area, Jilin province: Acta Petrologica Sinica, v. 18, no. 4, p. 495-500.

Fan, Q., Sun, Q., Li, N., Yin, J., Chen, H., Gao, F., and Zhang, X., 2003, The section of airfall clastic rock of Holocene volcano in Jingbohu region and its eruptive history: Seismology and Geology, v. 25, p. 3-11.

Feng, M., and Whitford-Stark, J., 1986, The 1719–1721 eruptions of potassium-rich lavas at Wudalianchi, China: Journal of volcanology and geothermal research, v. 30, no. 1-2, p. 131-148.

Finn, C. A., Müller, R. D., and Panter, K. S., 2005, A Cenozoic diffuse alkaline magmatic province (DAMP) in the southwest Pacific without rift or plume origin: Geochemistry, Geophysics, Geosystems, v. 6, no. 2.

Global Volcanism Program, 2013, Volcanoes of the World: Smithsonian Institution

Govers, R., and Wortel, M., 2005, Lithosphere tearing at STEP faults: Response to edges of subduction zones: Earth and Planetary Science Letters, v. 236, no. 1-2, p. 505-523.

Graham, D. W., Larsen, L., Hanan, B., Storey, M., Pedersen, A., and Lupton, J., 1998, Helium isotope composition of the early Iceland mantle plume inferred from the Tertiary picrites of West Greenland: Earth and Planetary Science Letters, v. 160, no. 3-4, p. 241-255.

Gvirtzman, Z., and Nur, A., 1999, The formation of Mount Etna as the consequence of slab rollback: Nature, v. 401, no. 6755, p. 782.

Hall, R., 2002, Cenozoic geological and plate tectonic evolution of SE Asia and the SW Pacific: computer-based reconstructions, model and animations: Journal of Asian Earth Sciences, v. 20, no. 4, p. 353-431.

Hall, R., and Spakman, W., 2015, Mantle structure and tectonic history of SE Asia: Tectonophysics, v. 658, p. 14-45.

Harbert, W., and Cox, A., 1989, Late Neogene motion of the Pacific plate: Journal of Geophysical Research: Solid Earth, v. 94, no. B3, p. 3052-3064.

Hawkesworth, C., Turner, S., McDermott, F., Peate, D., and Van Calsteren, P., 1997a, U-Th isotopes in arc magmas: Implications for element transfer from the subducted crust: Science, v. 276, no. 5312, p. 551-555.

Hawkesworth, C., Turner, S., Peate, D., McDermott, F., and Van Calsteren, P., 1997b, Elemental U and Th variations in island arc rocks: implications for U-series isotopes: Chemical Geology, v. 139, no. 1-4, p. 207-221.

Hayes, G., 2018, Slab2–A Comprehensive Subduction Zone Geometry Model: US Geological Survey data release.

Hayes, G. P., Moore, G. L., Portner, D. E., Hearne, M., Flamme, H., Furtney, M., and Smoczyk, G. M., 2018, Slab2, a comprehensive subduction zone geometry model: Science, v. 362, no. 6410, p. 58-61.

Heuret, A., and Lallemand, S., 2005, Plate motions, slab dynamics and back-arc deformation: Physics of the Earth and Planetary Interiors, v. 149, no. 1-2, p. 31-51.

Hickey-Vargas, R., 2005, Basalt and tonalite from the Amami Plateau, northern West Philippine Basin: New Early Cretaceous ages and geochemical results, and their petrologic and tectonic implications: Island Arc, v. 14, no. 4, p. 653-665.

Hilde, T. W., and Chao-Shing, L., 1984, Origin and evolution of the West Philippine Basin: a new interpretation: Tectonophysics, v. 102, no. 1-4, p. 85-104.

Hoang, N., Uto, K., Matsumoto, A., and Itoh, J. i., 2013, Pleistocene intraplate magmatism in the Goto Islands, SW Japan: implications for mantle source evolution and regional geodynamics: Journal of Geodynamics, v. 68, p. 1-17.

Hoffer, G., Eissen, J.-P., Beate, B., Bourdon, E., Fornari, M., and Cotten, J., 2008, Geochemical and petrological constraints on rear-arc magma genesis processes in Ecuador: The Puyo cones and Mera lavas volcanic formations: Journal of Volcanology and Geothermal Research, v. 176, no. 1, p. 107-118.

Horn, S., and Schmincke, H.-U., 2000, Volatile emission during the eruption of Baitoushan Volcano (China/North Korea) ca. 969 AD: Bulletin of Volcanology, v. 61, no. 8, p. 537-555.

Im, J. H., Shim, S. H., Choo, C. O., Jang, Y. D., and Lee, J. S., 2012, Volcanological and paleoenvironmental implications of charcoals of the Nari Formation in Nari Caldera, Ulleung Island, Korea: Geosciences Journal, v. 16, no. 2, p. 105-114.

Jolivet, L., Faccenna, C., Becker, T., Tesauro, M., Sternai, P., and Bouilhol, P., 2018, Mantle Flow and Deforming Continents: From India-Asia Convergence to Pacific Subduction: Tectonics, v. 37, no. 9, p. 2887-2914.

Jolliffe, I. T., and Cadima, J., 2016, Principal component analysis: a review and recent developments: Philosophical Transactions of the Royal Society A: Mathematical, Physical and Engineering Sciences, v. 374, no. 2065, p. 20150202.

Kim, H.-J., Han, S.-J., Lee, G. H., and Huh, S., 1998, Seismic study of the Ulleung Basin crust and its implications for the opening of the East Sea (Japan Sea): Marine Geophysical Researches, v. 20, no. 3, p. 219-237.

Kim, J.-I., Choi, S. H., Koh, G. W., Park, J. B., and Ryu, J.-S., 2019, Petrogenesis and mantle source characteristics of volcanic rocks on Jeju Island, South Korea: Lithos, v. 326, p. 476-490.

Kim, K. H., Nagao, K., Sumino, H., Tanaka, T., Hayashi, T., Nakamura, T., and Lee, J. I., 2008, He–Ar and Nd–Sr isotopic compositions of late Pleistocene felsic plutonic back arc basin rocks from Ulleungdo volcanic island, South Korea: Implications for the genesis of young plutonic rocks in a back arc basin: Chemical Geology, v. 253, no. 3-4, p. 180-195.

Kim, K. H., Tanaka, T., Nagao, K., and Jang, S. K., 1999, Nd and Sr isotopes and K-Ar ages of the Ulreungdo alkali volcanic rocks in the East Sea, South Korea: Geochemical Journal, v. 33, no. 5, p. 317-341.

Kimura, J.-I., Sakuyama, T., Miyazaki, T., Vaglarov, B. S., Fukao, Y., and Stern, R. J., 2018, Plume-stagnant slab-lithosphere interactions: Origin of the late Cenozoic intra-plate basalts on the East Eurasia margin: Lithos, v. 300, p. 227-249.

King, S. D., and Anderson, D. L., 1998, Edge-driven convection: Earth and Planetary Science Letters, v. 160, no. 3-4, p. 289-296.

Kita, I., Asakawa, Y., Yuri, T., Yasui, M., Shimoike, Y., Yamamoto, M., Hasegawa, H., Taguchi, S., and Sumino, H., 2012, Rifting of Kyushu, Japan, based on the fault-controlled concurrent eruption of oceanic island basalt-type and island arc-type lavas: Bulletin of volcanology, v. 74, no. 5, p. 1121-1139.

Kita, I., Yamamoto, M., Asakawa, Y., Nakagawa, M., Taguchi, S., and Hasegawa, H., 2001, Contemporaneous ascent of within-plate type and island-arc type magmas in the Beppu–Shimabara graben system, Kyushu island, Japan: Journal of Volcanology and Geothermal Research, v. 111, no. 1, p. 99-109.

Kuritani, T., Ohtani, E., and Kimura, J.-I., 2011, Intensive hydration of the mantle transition zone beneath China caused by ancient slab stagnation: Nature Geoscience, v. 4, no. 10, p. 713.

Kuritani, T., Tanaka, M., Yokoyama, T., Nakagawa, M., and Matsumoto, A., 2016, Intensive hydration of the wedge mantle at the Kuril Arc–NE Japan Arc junction: implications from mafic lavas from Usu Volcano, northern Japan: Journal of petrology, v. 57, no. 6, p. 1223-1240.

Lallemand, S., 2016, Philippine Sea Plate inception, evolution, and consumption with special emphasis on the early stages of Izu-Bonin-Mariana subduction: Progress in Earth and Planetary Science, v. 3, no. 1, p. 15.

Li, C., Van Der Hilst, R. D., Engdahl, E. R., and Burdick, S., 2008, A new global model for P wave speed variations in Earth's mantle: Geochemistry, Geophysics, Geosystems, v. 9, no. 5.

Li, S.-G., Yang, W., Ke, S., Meng, X., Tian, H., Xu, L., He, Y., Huang, J., Wang, X.-C., and Xia, Q., 2017, Deep carbon cycles constrained by a large-scale mantle Mg isotope anomaly in eastern China: National Science Review, v. 4, no. 1, p. 111-120.

Lin, J. Y., Hsu, S. K., and Sibuet, J. C., 2004, Melting features along the Ryukyu slab tear, beneath the southwestern Okinawa Trough: Geophysical Research Letters, v. 31, no. 19.

Liu, X., Zhao, D., Li, S., and Wei, W., 2017, Age of the subducting Pacific slab beneath East Asia and its geodynamic implications: Earth and Planetary Science Letters, v. 464, p. 166-174.

Mather, B. R., Müller, R. D., Seton, M., Ruttor, S., Nebel, O., and Mortimer, N., 2020, Intraplate volcanism triggered by bursts in slab flux: Science Advances, v. 6, no. 51, p. eabd0953.

McCulloch, M. T., and Gamble, J., 1991, Geochemical and geodynamical constraints on subduction zone magmatism: Earth and Planetary Science Letters, v. 102, no. 3-4, p. 358-374.

McGee, L. E., McLeod, C., and Davidson, J. P., 2015, A spectrum of disequilibrium melting preserved in lava-hosted, partially melted crustal xenoliths from the Wudalianchi volcanic field, NE China: Chemical Geology, v. 417, p. 184-199.

Meng, F.-c., Safonova, I., Chen, S.-s., and Ribeal, P., 2018, Late Cenozoic intra-plate basalts of the Greater Khingan Range in NE China and Khangai Province in Central Mongolia: Gondwana Research, v. 63, p. 65-84.

Miyoshi, M., Fukuoka, T., Sano, T., and Hasenaka, T., 2008, Subduction influence of Philippine Sea plate on the mantle beneath northern Kyushu, SW Japan: An examination of boron contents in basaltic rocks: Journal of volcanology and geothermal research, v. 171, no. 1, p. 73-87.

Montelli, R., Nolet, G., Dahlen, F., Masters, G., Engdahl, E. R., and Hung, S.-H., 2004, Finite-frequency tomography reveals a variety of plumes in the mantle: Science, v. 303, no. 5656, p. 338-343.

Moyen, J.-F., 2009, High Sr/Y and La/Yb ratios: the meaning of the "adakitic signature": Lithos, v. 112, no. 3-4, p. 556-574.

Müller, R. D., Sdrolias, M., Gaina, C., and Roest, W. R., 2008, Age, spreading rates, and spreading asymmetry of the world's ocean crust: Geochemistry, Geophysics, Geosystems, v. 9, no. 4.

Nakajima, J., and Hasegawa, A., 2007, Subduction of the Philippine Sea plate beneath southwestern Japan: Slab geometry and its relationship to arc magmatism: Journal of Geophysical Research: Solid Earth, v. 112, no. B8.

Nelson, P. L., and Grand, S. P., 2018, Lower-mantle plume beneath the Yellowstone hotspot revealed by core waves: Nature Geoscience, v. 11, no. 4, p. 280-284.

Nolet, G., Allen, R., and Zhao, D., 2007, Mantle plume tomography: Chemical Geology, v. 241, no. 3-4, p. 248-263.

Okada, S., and Ikeda, Y., 2012, Quantifying crustal extension and shortening in the back-arc region of northeast Japan: Journal of Geophysical Research: Solid Earth, v. 117, no. B1.

Okino, K., Kasuga, S., and Ohara, Y., 1998, A new scenario of the Parece Vela Basin genesis: Marine Geophysical Researches, v. 20, no. 1, p. 21-40.

Perfit, M. R., and Davidson, J. P., 2000, Plate tectonics and volcanism: Encyclopedia of Volcanoes, p. 89-113.

Pownall, J. M., Lister, G. S., and Spakman, W., 2017, Reconstructing subducted oceanic lithosphere by "reverse-engineering" slab geometries: The northern Philippine Sea Plate: Tectonics, v. 36, no. 9, p. 1814-1834.

Qicheng, F., Qian, S., Ni, L., and Tuanhua, W., 2006, Holocene volcanic rocks in Jingbo Lake region Deversity of magmatism: Progress in Natural Science, v. 16, no. 1, p. 65-72.

R Core Team, 2013, R: A language and environment for statistical computing, Vienna, Austria.

Ringnér, M., 2008, What is principal component analysis?: Nature biotechnology, v. 26, no. 3, p. 303-304.

Rosenbaum, G., Gasparon, M., Lucente, F. P., Peccerillo, A., and Miller, M. S., 2008, Kinematics of slab tear faults during subduction segmentation and implications for Italian magmatism: Tectonics, v. 27, no. 2.

Rosenbaum, G., Sandiford, M., Caulfield, J., and Garrison, J. M., 2018, A trapdoor mechanism for slab tearing and melt generation in the northern Andes: Geology.

Sato, H., and Amano, K., 1991, Relationship between tectonics, volcanism, sedimentation and basin development, Late Cenozoic, central part of Northern Honshu, Japan: Sedimentary geology, v. 74, no. 1-4, p. 323-343.

Schellart, W., 2010, Mount Etna–Iblean volcanism caused by rollback-induced upper mantle upwelling around the Ionian slab edge: an alternative to the plume model: Geology, v. 38, no. 8, p. 691-694.

Schellart, W. P., and Lister, G., 2005, The role of the East Asian active margin in widespread extensional and strike-slip deformation in East Asia: Journal of the Geological Society, v. 162, no. 6, p. 959-972.

Schmidt, M. W., and Poli, S., 1998, Experimentally based water budgets for dehydrating slabs and consequences for arc magma generation: Earth and Planetary Science Letters, v. 163, no. 1-4, p. 361-379.

Seton, M., Müller, R., Zahirovic, S., Gaina, C., Torsvik, T., Shephard, G., Talsma, A., Gurnis, M., Turner, M., and Maus, S., 2012, Global continental and ocean basin reconstructions since 200 Ma: Earth-Science Reviews, v. 113, no. 3-4, p. 212-270.

Shibata, T., Yoshikawa, M., Ujike, O., Miyoshi, M., and Takemura, K., 2014, Along-arc geochemical variations in Quaternary magmas of northern Kyushu Island, Japan: Geological Society, London, Special Publications, v. 385, no. 1, p. 15-29.

Sibuet, J. C., Deffontaines, B., Hsu, S. K., Thareau, N., Le Formal, J. P., and Liu, C. S., 1998, Okinawa trough backarc basin: Early tectonic and magmatic evolution: Journal of Geophysical Research: Solid Earth, v. 103, no. B12, p. 30245-30267.

Simutė, S., Steptoe, H., Cobden, L., Gokhberg, A., and Fichtner, A., 2016, Full-waveform inversion of the Japanese Islands region: Journal of Geophysical Research: Solid Earth, v. 121, no. 5, p. 3722-3741.

Sohn, Y., and Yoon, S.-H., 2010, Shallow-marine records of pyroclastic surges and fallouts over water in Jeju Island, Korea, and their stratigraphic implications: Geology, v. 38, no. 8, p. 763-766.

Sohn, Y. K., and Park, K. H., 2004, Early-stage volcanism and sedimentation of Jeju Island revealed by the Sagye borehole, SW Jeju Island, Korea: Geosciences Journal, v. 8, no. 1, p. 73.

Song, J. H., Kim, S., Rhie, J., Lee, S. H., Kim, Y., and Kang, T. S., 2018, Imaging of lithospheric structure beneath Jeju Volcanic Island by teleseismic traveltime tomography: Journal of Geophysical Research: Solid Earth, v. 123, no. 8, p. 6784-6801.

Strak, V., and Schellart, W. P., 2014, Evolution of 3-D subduction-induced mantle flow around lateral slab edges in analogue models of free subduction analysed by stereoscopic particle image velocimetry technique: Earth and Planetary Science Letters, v. 403, p. 368-379.

Sugimoto, T., Shibata, T., Yoshikawa, M., and Takemura, K., 2006, Sr-Nd-Pb isotopic and major and trace element compositions of the Yufu-Tsurumi volcanic rocks: implications for the

magma genesis of the Yufu-Tsurumi volcanoes, northeast Kyushu, Japan: Journal of Mineralogical and Petrological Sciences, v. 101, no. 5, p. 270-275.

Sun, C. H., and Stern, R. J., 2001, Genesis of Mariana shoshonites: Contribution of the subduction component: Journal of Geophysical Research: Solid Earth, v. 106, no. B1, p. 589-608.

Sun, S.-S., and McDonough, W.-S., 1989, Chemical and isotopic systematics of oceanic basalts: implications for mantle composition and processes: Geological Society, London, Special Publications, v. 42, no. 1, p. 313-345.

Sun, Y., Teng, F. Z., Ying, J. F., Su, B. X., Hu, Y., Fan, Q. C., and Zhou, X. H., 2017, Magnesium Isotopic Evidence for Ancient Subducted Oceanic Crust in LOMU-Like Potassium-Rich Volcanic Rocks: Journal of Geophysical Research: Solid Earth, v. 122, no. 10, p. 7562-7572.

Sun, Y., Ying, J., Zhou, X., Shao, J. a., Chu, Z., and Su, B., 2014, Geochemistry of ultrapotassic volcanic rocks in Xiaogulihe NE China: Implications for the role of ancient subducted sediments: Lithos, v. 208, p. 53-66.

Tang, Y., Obayashi, M., Niu, F., Grand, S. P., Chen, Y. J., Kawakatsu, H., Tanaka, S., Ning, J., and Ni, J. F., 2014, Changbaishan volcanism in northeast China linked to subduction-induced mantle upwelling: Nature Geoscience, v. 7, no. 6, p. 470.

Tao, K., Grand, S. P., and Niu, F., 2018, Seismic structure of the upper mantle beneath Eastern Asia from full waveform seismic tomography: Geochemistry, Geophysics, Geosystems, v. 19, no. 8, p. 2732-2763.

Tatsumi, Y., Shukuno, H., Yoshikawa, M., Chang, Q., Sato, K., and Lee, M. W., 2004, The petrology and geochemistry of volcanic rocks on Jeju Island: plume magmatism along the Asian continental margin: Journal of Petrology, v. 46, no. 3, p. 523-553.

Uto, K., and Tatsumi, Y., 1996, Quaternary volcanism of the Japanese Islands: Island Arc, v. 5, no. 3, p. 250-261.

van der Meer, D. G., van Hinsbergen, D. J., and Spakman, W., 2018, Atlas of the underworld: Slab remnants in the mantle, their sinking history, and a new outlook on lower mantle viscosity: Tectonophysics, v. 723, p. 309-448.

Verma, S. P., 2002, Absence of Cocos plate subduction-related basic volcanism in southern Mexico: A unique case on Earth?: Geology, v. 30, no. 12, p. 1095-1098.

Wang, X.-J., Chen, L.-H., Hofmann, A. W., Mao, F.-G., Liu, J.-Q., Zhong, Y., Xie, L.-W., and Yang, Y.-H., 2017, Mantle transition zone-derived EM1 component beneath NE China: Geochemical evidence from Cenozoic potassic basalts: Earth and Planetary Science Letters, v. 465, p. 16-28.

Wang, Y., Li, C., Wei, H., and Shan, X., 2003, Late Pliocene–recent tectonic setting for the Tianchi volcanic zone, Changbai Mountains, northeast China: Journal of Asian Earth Sciences, v. 21, no. 10, p. 1159-1170.

Wei, H., Wang, Y., Jin, J., Gao, L., Yun, S.-H., and Jin, B., 2007, Timescale and evolution of the intracontinental Tianchi volcanic shield and ignimbrite-forming eruption, Changbaishan, Northeast China: Lithos, v. 96, no. 1-2, p. 315-324.

Wei, W., Xu, J., Zhao, D., and Shi, Y., 2012, East Asia mantle tomography: New insight into plate subduction and intraplate volcanism: Journal of Asian Earth Sciences, v. 60, p. 88-103.

Wessel, P., and Kroenke, L. W., 2000, Ontong Java Plateau and late Neogene changes in Pacific plate motion: Journal of Geophysical Research: Solid Earth, v. 105, no. B12, p. 28255-28277.

Weston, J., Engdahl, E., Harris, J., Di Giacomo, D., and Storchak, D., 2018, ISC-EHB: reconstruction of a robust earthquake data set: Geophysical Journal International, v. 214, no. 1, p. 474-484.

Wickham, H., 2016, ggplot2: elegant graphics for data analysis, springer.

Wickham, H., Averick, M., Bryan, J., Chang, W., McGowan, L. D. A., François, R., Grolemund, G., Hayes, A., Henry, L., and Hester, J., 2019, Welcome to the Tidyverse: Journal of Open Source Software, v. 4, no. 43, p. 1686.

Wu, J., Suppe, J., Lu, R., and Kanda, R., 2016, Philippine Sea and East Asian plate tectonics since 52 Ma constrained by new subducted slab reconstruction methods: Journal of Geophysical Research: Solid Earth, v. 121, no. 6, p. 4670-4741.

Xia, S., Zhao, D., Sun, J., and Huang, H., 2016, Teleseismic imaging of the mantle beneath southernmost China: New insights into the Hainan plume: Gondwana Research, v. 36, p. 46-56.

Xu, Y.-G., Menzies, M. A., Thirlwall, M. F., Huang, X.-L., Liu, Y., and Chen, X.-M., 2003, "Reactive" harzburgites from Huinan, NE China: products of the lithosphere-asthenosphere interaction during lithospheric thinning?: Geochimica et Cosmochimica Acta, v. 67, no. 3, p. 487-505.

Xu, Z., and Zheng, Y.-F., 2017, Continental basalts record the crust-mantle interaction in oceanic subduction channel: A geochemical case study from eastern China: Journal of Asian Earth Sciences, v. 145, p. 233-259.

Xu, Z.-h., 2001, A present-day tectonic stress map for eastern Asia region: Acta Seismologica Sinica, v. 14, no. 5, p. 524-533.

Yamazaki, T., Takahashi, M., Iryu, Y., Sato, T., Oda, M., Takayanagi, H., Chiyonobu, S., Nishimura, A., Nakazawa, T., and Ooka, T., 2010, Philippine Sea Plate motion since the Eocene estimated from paleomagnetism of seafloor drill cores and gravity cores: Earth, planets and space, v. 62, no. 6, p. 495-502.

Yang, J., and Faccenda, M., 2020, Intraplate volcanism originating from upwelling hydrous mantle transition zone: Nature, v. 579, no. 7797, p. 88-91.

Yang, W., Teng, F.-Z., Zhang, H.-F., and Li, S.-G., 2012, Magnesium isotopic systematics of continental basalts from the North China craton: Implications for tracing subducted carbonate in the mantle: Chemical Geology, v. 328, p. 185-194.

Yarmolyuk, V., Savatenkov, V., Stupak, F. and Kudryashova, E., Sources of Magmas and Conditions of Rock Formation in the Late Cenozoic Udokan Volcanic Plateau, *in* Proceedings Doklady Earth Sciences2020, Volume 493, Springer, p. 517-521.

Yarmolyuk, V. V., Kudryashova, E. A., Kozlovsky, A. M., Lebedev, V. A., and Savatenkov, V. M., 2015, Late Mesozoic–Cenozoic intraplate magmatism in Central Asia and its relation with mantle diapirism: Evidence from the South Khangai volcanic region, Mongolia: Journal of Asian Earth Sciences, v. 111, p. 604-623.

Yi, S., Yun, H., and Yoon, S., 1998, Calcareous nannoplankton from the Seoguipo Formation of Cheju Island, Korea and its paleoceanographic implications: Paleontological Research, v. 2, no. 4, p. 253-265.

Yokoyama, T., Kuritani, T., Kobayashi, K., and Nakamura, E., 2006, Geochemical evolution of a shallow magma plumbing system during the last 500 years, Miyakejima volcano, Japan: constraints from 238 U–230 Th–226 Ra systematics: Geochimica et cosmochimica acta, v. 70, no. 11, p. 2885-2901.

Yu, H., Zhao, L., Liu, Y., Ning, J., Chen, Q.-F., and Lin, J., 2016, Stress adjustment revealed by seismicity and earthquake focal mechanisms in northeast China before and after the 2011 Tohoku-Oki earthquake: Tectonophysics, v. 666, p. 23-32.

Zhang, L.-Y., Prelević, D., Li, N., Mertz-Kraus, R., and Buhre, S., 2016, Variation of olivine composition in the volcanic rocks in the Songliao basin, NE China: lithosphere control on the origin of the K-rich intraplate mafic lavas: Lithos, v. 262, p. 153-168.

Zhang, M., Guo, Z., Liu, J., Liu, G., Zhang, L., Lei, M., Zhao, W., Ma, L., Sepe, V., and Ventura, G., 2018, The intraplate Changbaishan volcanic field (China/North Korea): A review on eruptive history, magma genesis, geodynamic significance, recent dynamics and potential hazards: Earth-Science Reviews, v. 187, p. 19-52.

Zhang, M., Suddaby, P., Thompson, R. N., Thirlwall, M. F., and Menzies, M. A., 1995, Potassic volcanic rocks in NE China: geochemical constraints on mantle source and magma genesis: Journal of Petrology, v. 36, no. 5, p. 1275-1303.

Zhao, D., Maruyama, S., and Omori, S., 2007, Mantle dynamics of Western Pacific and East Asia: Insight from seismic tomography and mineral physics: Gondwana Research, v. 11, no. 1-2, p. 120-131.

Zheng, Y.-F., Xu, Z., Chen, L., Dai, L.-Q., and Zhao, Z.-F., 2020, Chemical geodynamics of mafic magmatism above subduction zones: Journal of Asian Earth Sciences, v. 194, p. 104185.

Zou, H., and Fan, Q., 2010, U–Th isotopes in Hainan basalts: Implications for sub-asthenospheric origin of EM2 mantle endmember and the dynamics of melting beneath Hainan Island: Lithos, v. 116, no. 1-2, p. 145-152.

Zou, H., Fan, Q., and Yao, Y., 2008, U–Th systematics of dispersed young volcanoes in NE China: asthenosphere upwelling caused by piling up and upward thickening of stagnant Pacific slab: Chemical Geology, v. 255, no. 1, p. 134-142.

Zou, H., Reid, M. R., Liu, Y., Yao, Y., Xu, X., and Fan, Q., 2003, Constraints on the origin of historic potassic basalts from northeast China by U–Th disequilibrium data: Chemical Geology, v. 200, no. 1-2, p. 189-201.

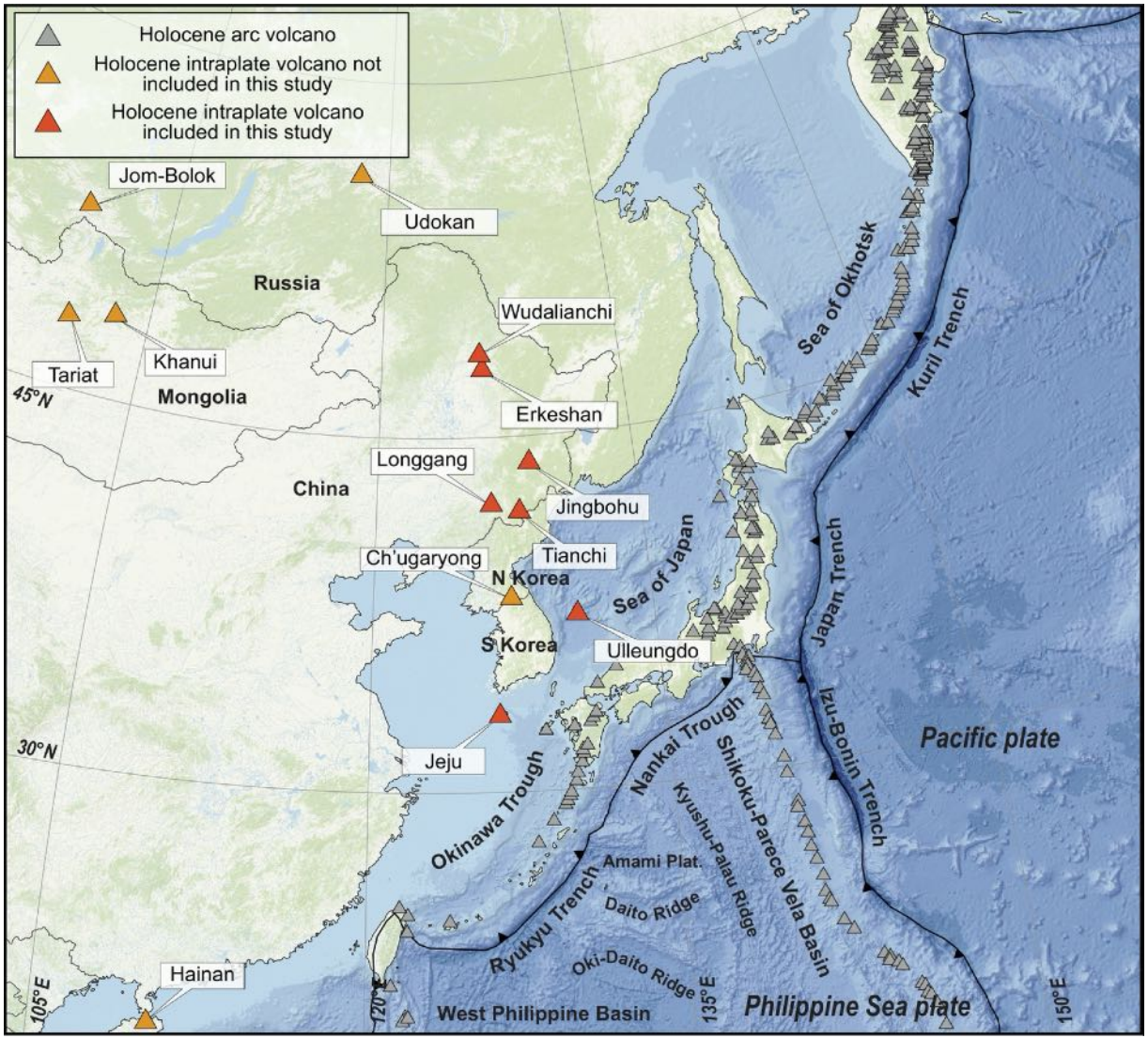
Holocene arc volcano
Holocene intraplate volcano not included in this study
Holocene intraplate volcano included in this study
Jom-Bolok
Udokan
Russia
Wudalianchi
Khanui
Tariat
Mongolia
45°N
Erkeshan
Longgang
China
Jingbohu
Ch'ugaryong
Tianchi
N Korea
S Korea
Ulleungdo
Jeju
30°N
Hainan
105°E
120°
135°E
150°E
Sea of Okhotsk
Kuril Trench
Sea of Japan
Japan Trench
Izu-Bonin Trench
Pacific plate
Okinawa Trough
Nankai Trough
Shikoku-Parece Vela Basin
Kyushu-Palau Ridge
Amami Plat.
Daito Ridge
Ryukyu Trench
Oki-Daito Ridge
West Philippine Basin
Philippine Sea plate

Figure 1

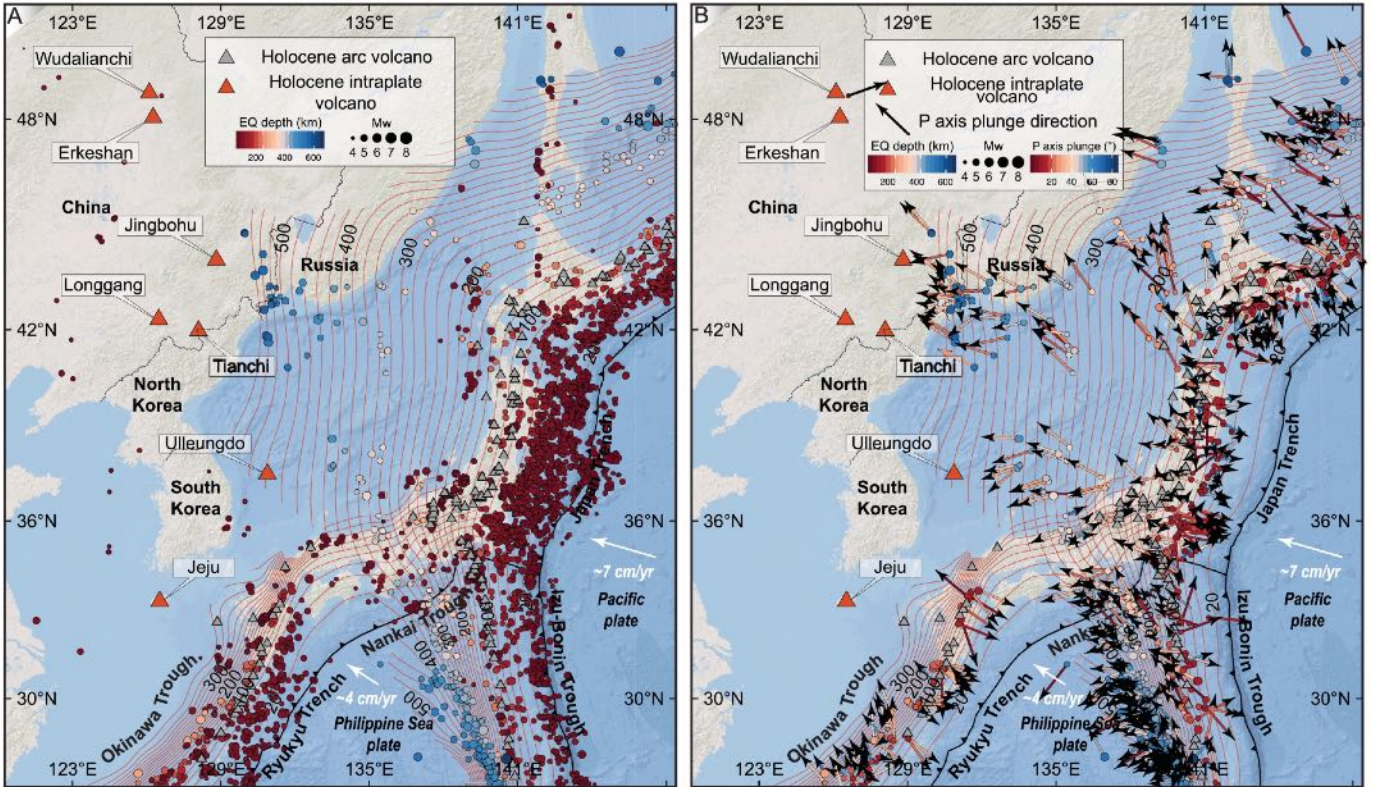
A
B
123°E
129°E
135°E
141°E
48°N
42°N
36°N
30°N
Wudalianchi
Erkeshan
Jingbohu
Longgang
Tianchi
Ulleungdo
Jeju
China
Russia
North Korea
South Korea
Holocene arc volcano
Holocene intraplate volcano
P axis plunge direction
EQ depth (km)
Mw
P axis plunge (°)
Japan Trench
Izu Bonin Trough
Nankai Trough
Ryukyu Trench
Okinawa Trough
~7 cm/yr
Pacific plate
~4 cm/yr
Philippine Sea plate

Figure 2

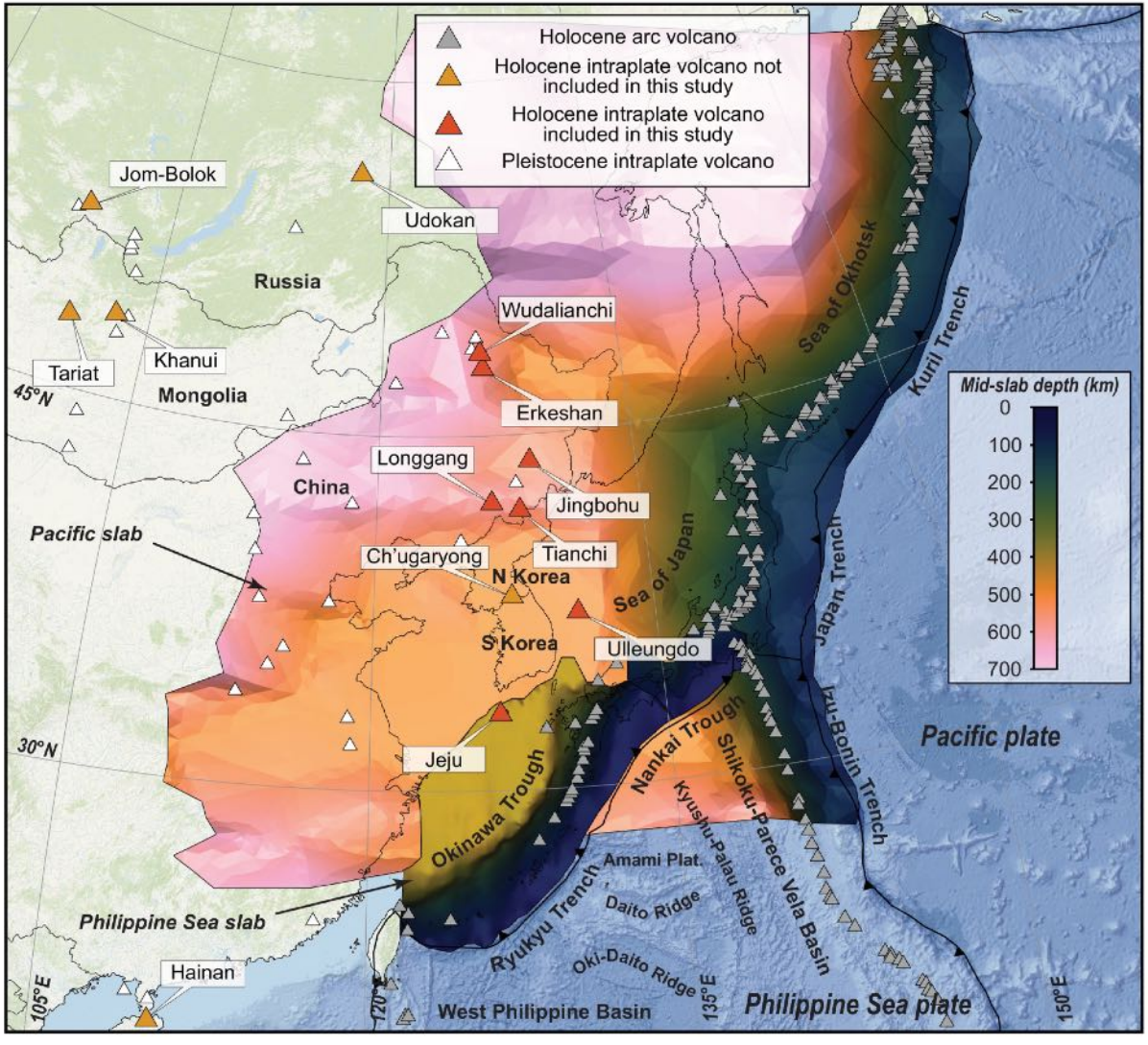
Holocene arc volcano
Holocene intraplate volcano not included in this study
Holocene intraplate volcano included in this study
Pleistocene intraplate volcano
Jom-Bolok
Udokan
Russia
Wudalianchi
Tariat
Khanui
Mongolia
45°N
Erkeshan
Longgang
China
Jingbohu
Pacific slab
Ch'ugaryong
Tianchi
N Korea
S Korea
Ulleungdo
Jeju
30°N
Philippine Sea slab
Hainan
105°E
120°
West Philippine Basin
135°E
150°E
Philippine Sea plate
Pacific plate
Sea of Okhotsk
Kuril Trench
Sea of Japan
Japan Trench
Izu-Bonin Trench
Nankai Trough
Shikoku-Parece Vela Basin
Kyushu-Palau Ridge
Okinawa Trough
Amami Plat.
Daito Ridge
Ryukyu Trench
Oki-Daito Ridge
Mid-slab depth (km)
0
100
200
300
400
500
600
700

Figure 3

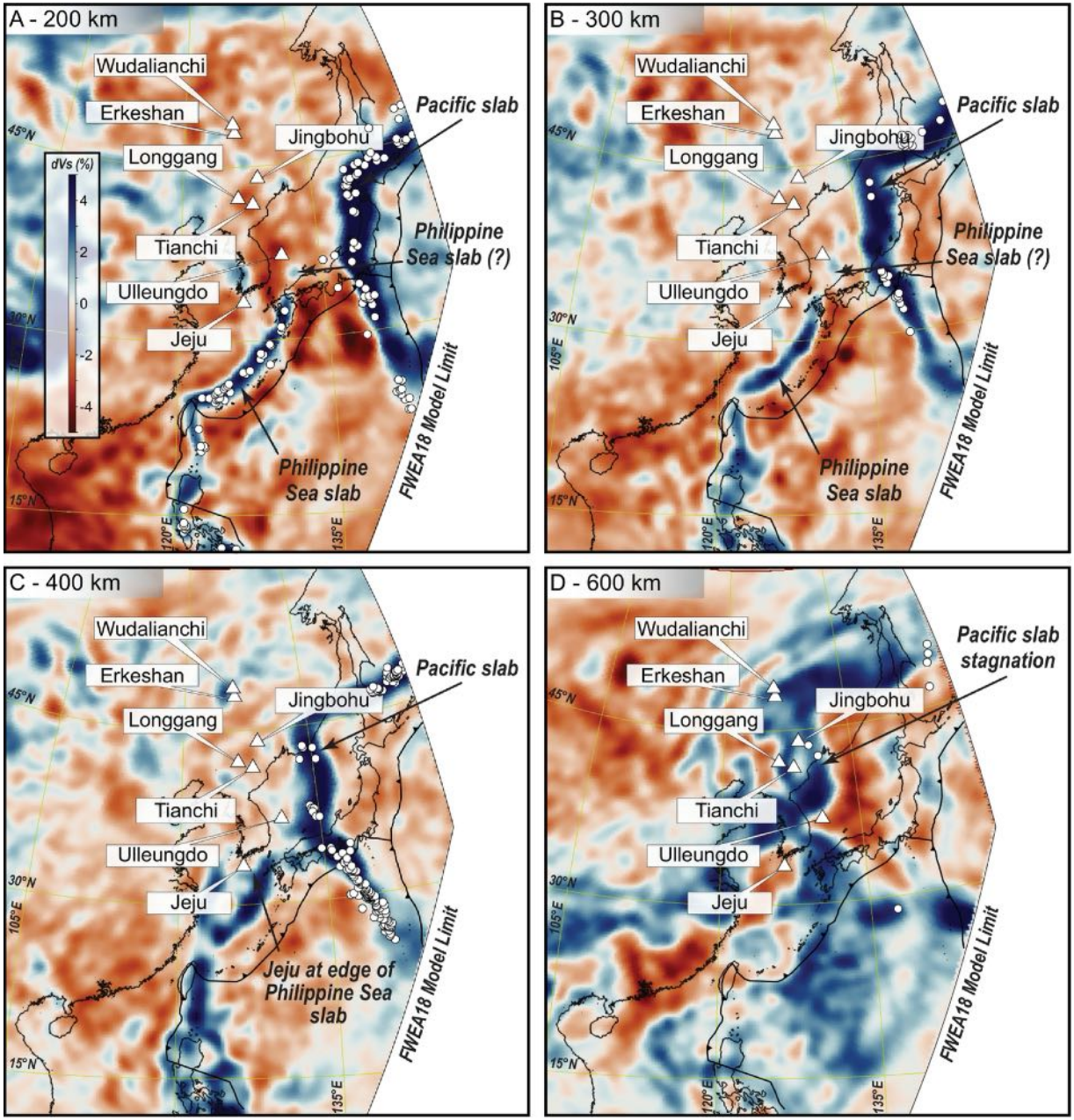
A - 200 km
B - 300 km
C - 400 km
D - 600 km
Wudalianchi
Erkeshan
Jingbohu
Longgang
Tianchi
Ulleungdo
Jeju
Pacific slab
Philippine Sea slab (?)
Philippine Sea slab
FWEA18 Model Limit
Jeju at edge of Philippine Sea slab
Pacific slab stagnation
dVs (%)
4
2
0
-2
-4
45°N
30°N
15°N
105°E
120°E
135°E

Figure 4

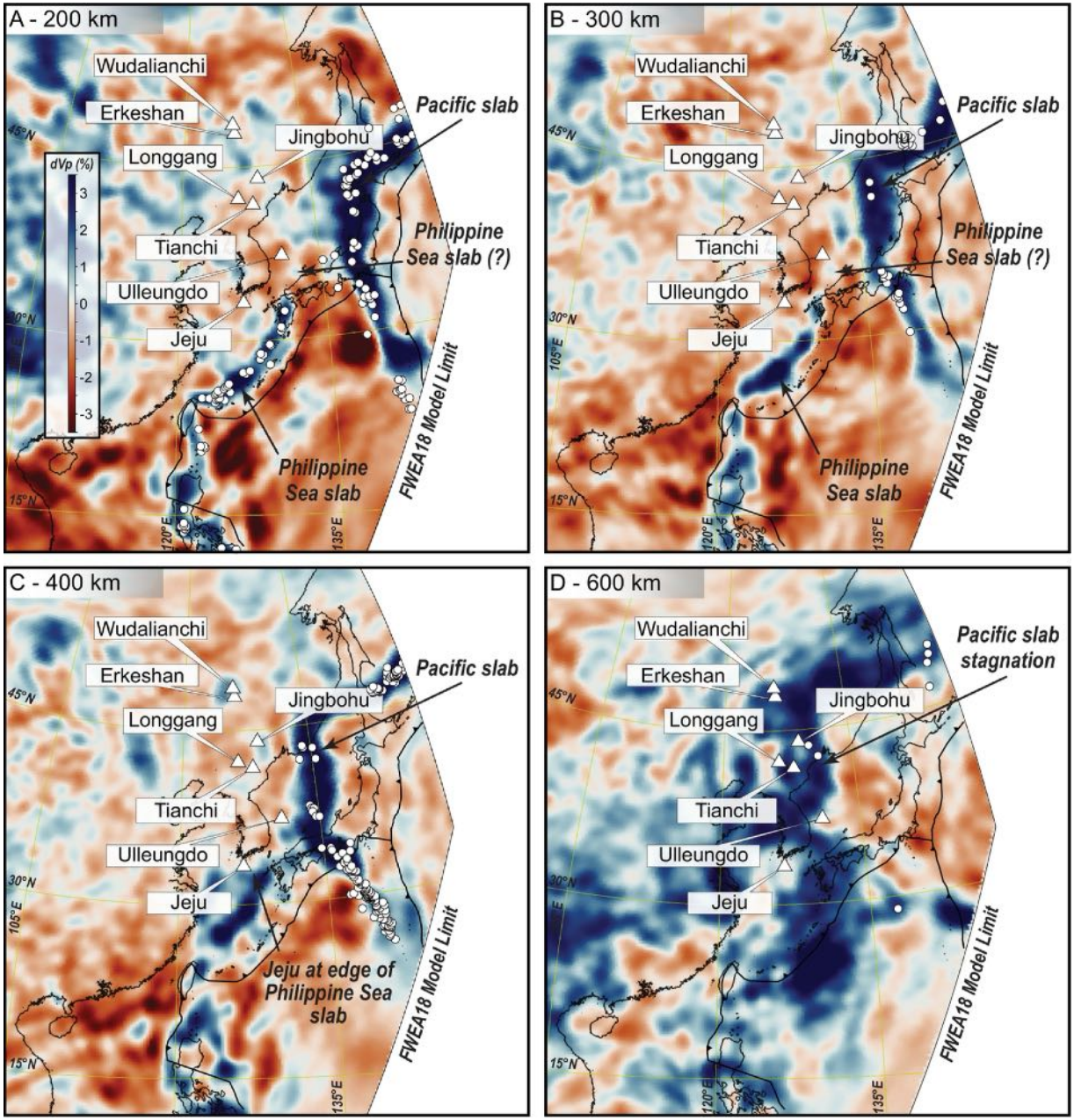
A - 200 km
B - 300 km
C - 400 km
D - 600 km
Wudalianchi
Erkeshan
Jingbohu
Longgang
Tianchi
Ulleungdo
Jeju
dVp (%)
3
2
1
0
-1
-2
-3
Pacific slab
Philippine Sea slab (?)
Philippine Sea slab
Jeju at edge of Philippine Sea slab
Pacific slab stagnation
FWEA18 Model Limit
45°N
30°N
15°N
105°E
120°E
135°E

Figure 5

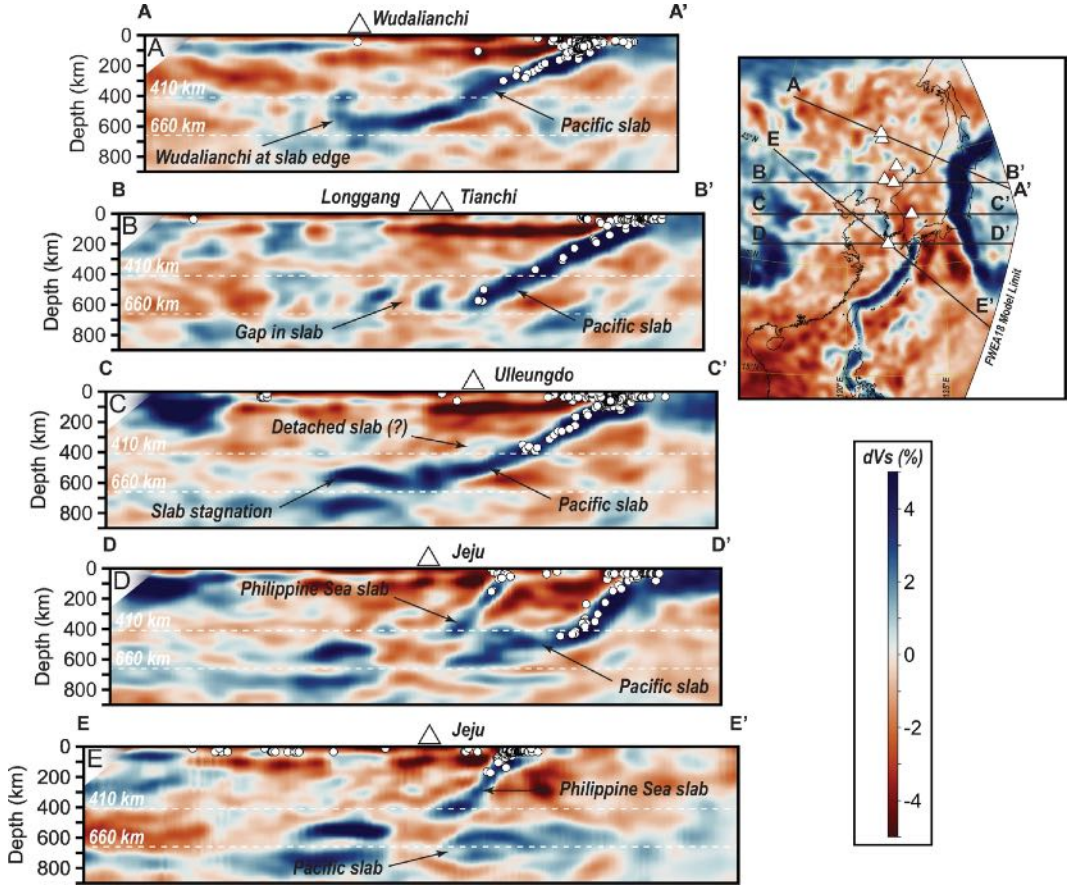
A
A'
Wudalianchi
Depth (km)
410 km
660 km
Pacific slab
Wudalianchi at slab edge
B
B'
Longgang
Tianchi
Gap in slab
Pacific slab
C
C'
Ulleungdo
Detached slab (?)
Slab stagnation
Pacific slab
D
D'
Jeju
Philippine Sea slab
Pacific slab
E
E'
Jeju
Philippine Sea slab
Pacific slab
PWEA18 Model Limit
dVs (%)
4
2
0
-2
-4

Figure 6

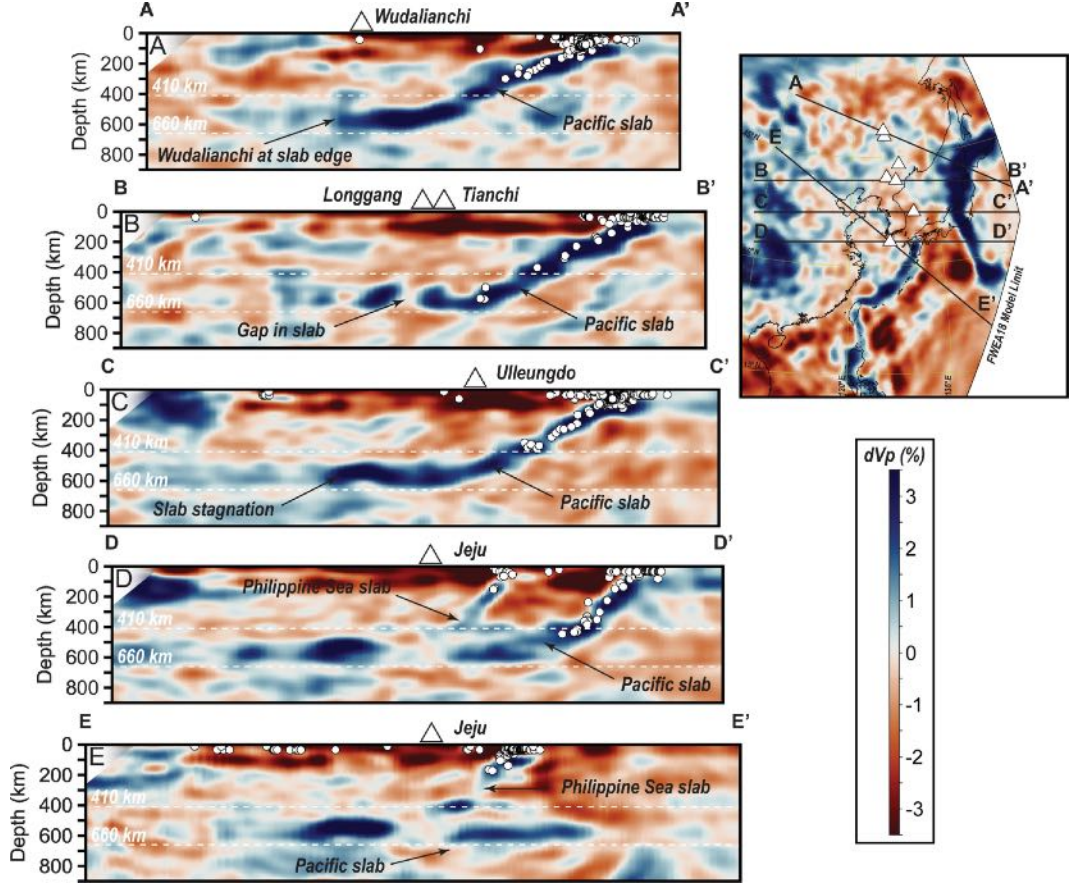
A
A'
Wudalianchi
Depth (km)
410 km
660 km
Pacific slab
Wudalianchi at slab edge
B
B'
Longgang
Tianchi
Gap in slab
C
C'
Ulleungdo
Slab stagnation
D
D'
Jeju
Philippine Sea slab
E
E'
PVEA13 Model Limit
dVp (%)
3
2
1
0
-1
-2
-3

Figure 7

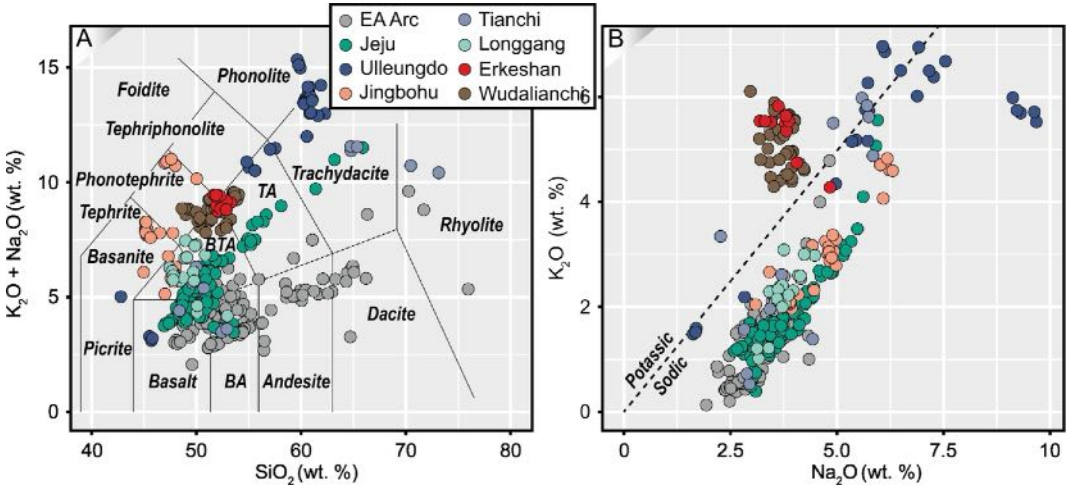
A
B
EA Arc
Jeju
Ulleungdo
Jingbohu
Tianchi
Longgang
Erkeshan
Wudalianchi
Foidite
Phonolite
Tephriphonolite
Phonotephrite
Tephrite
Basanite
Picrite
Basalt
BA
Andesite
Dacite
Trachydacite
Rhyolite
TA
BTA
$K_2O + Na_2O$ (wt. %)
SiO_2 (wt. %)
K_2O (wt. %)
Na_2O (wt. %)
Potassic
Sodic

Figure 8

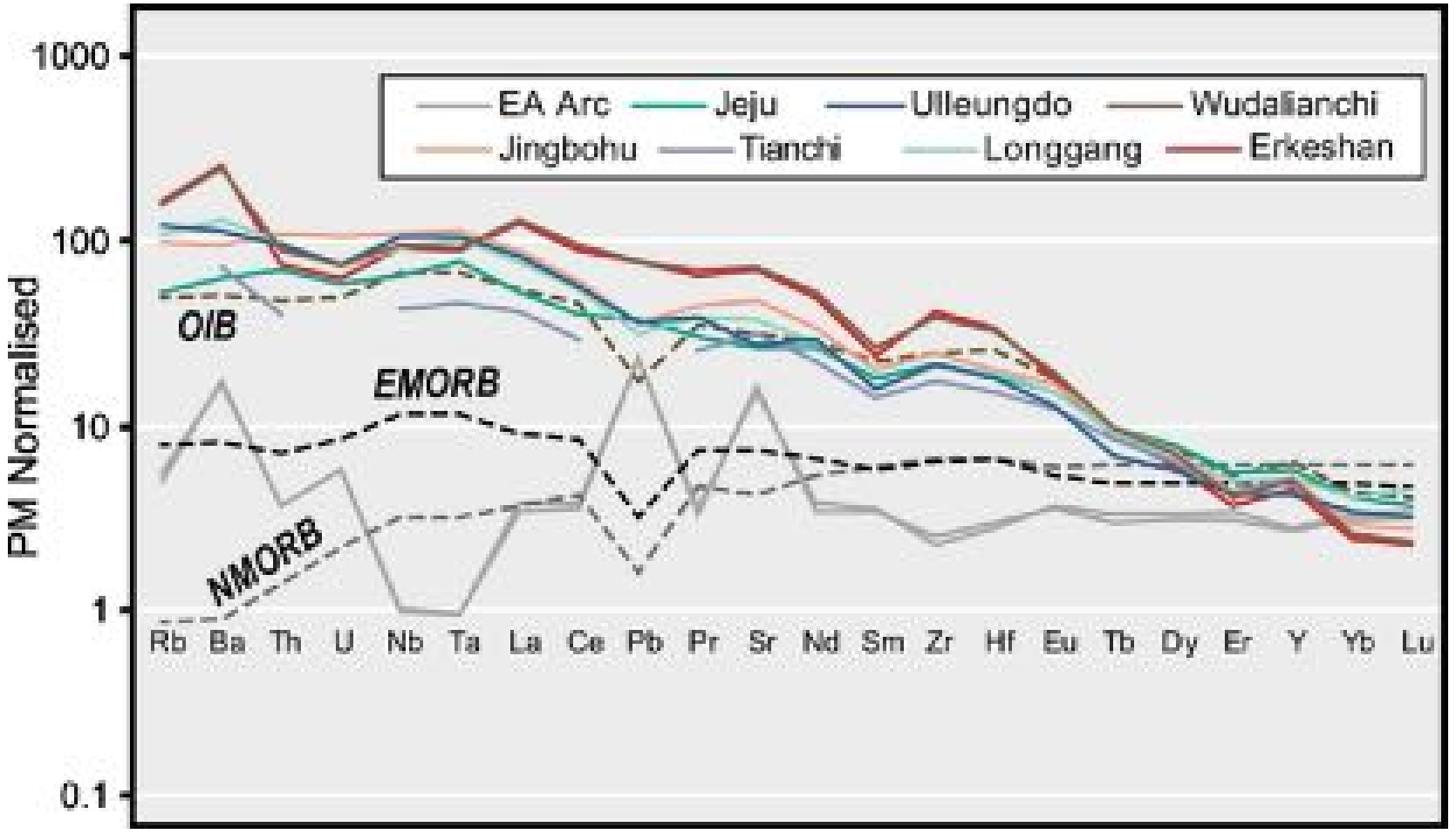
1000
100
10
1
0.1
PM Normalised
EA Arc
Jeju
Ulleungdo
Wudalianchi
Jingbohu
Tianchi
Longgang
Erkeshan
OIB
EMORB
NMORB
Rb Ba Th U Nb Ta La Ce Pb Pr Sr Nd Sm Zr Hf Eu Tb Dy Er Y Yb Lu

Figure 9

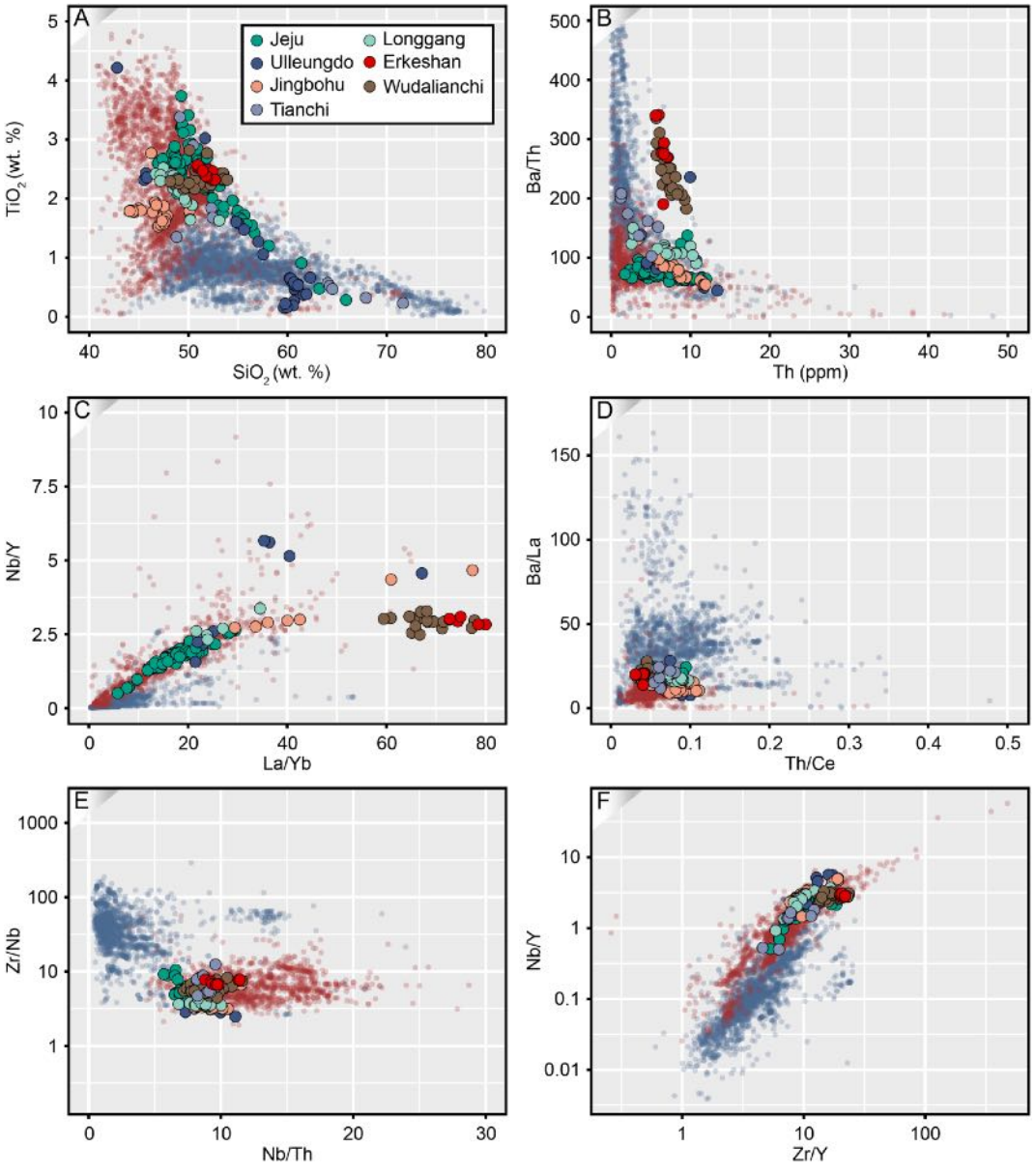
A
Jeju
Ulleungdo
Jingbohu
Tianchi
Longgang
Erkeshan
Wudalianchi
TiO2 (wt. %)
SiO2 (wt. %)
B
Ba/Th
Th (ppm)
C
Nb/Y
La/Yb
D
Ba/La
Th/Ce
E
Zr/Nb
Nb/Th
F
Nb/Y
Zr/Y

Figure 10

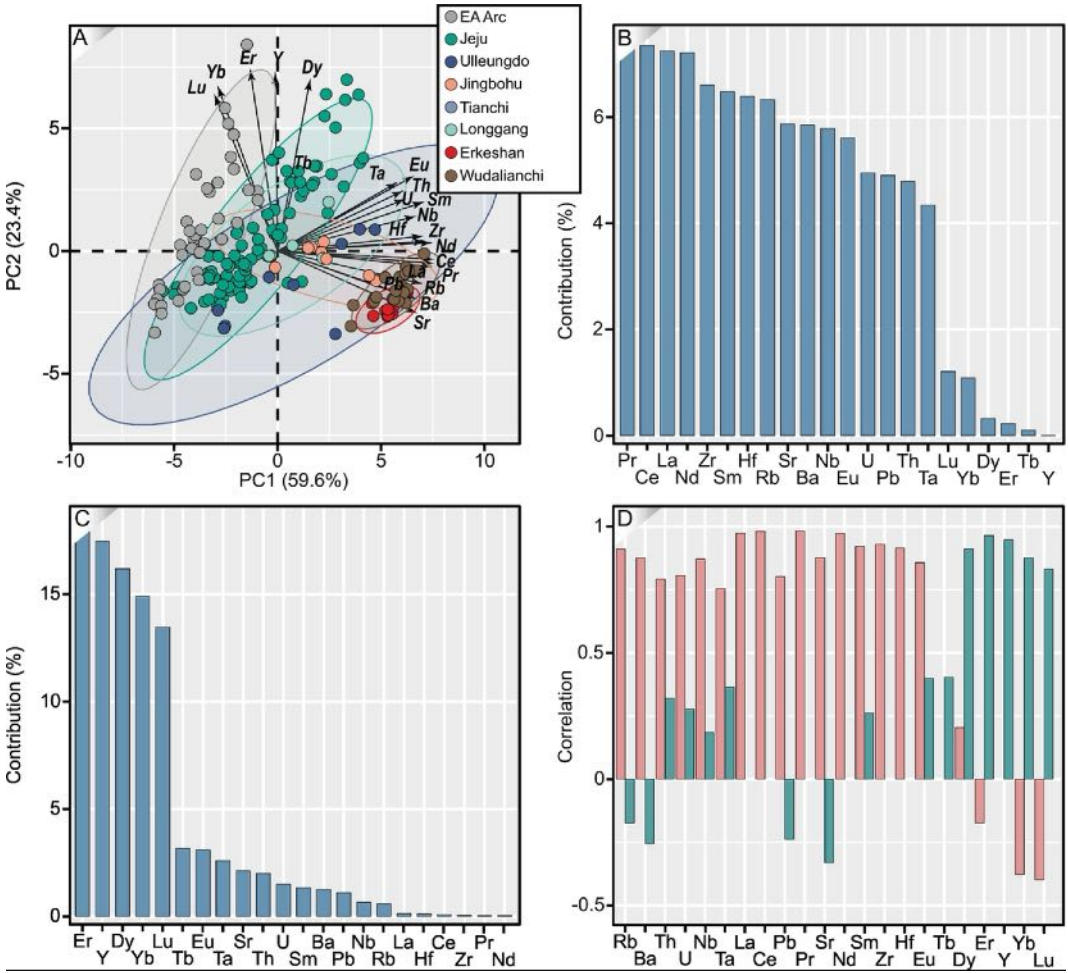
A
EA Arc
Jeju
Ulleungdo
Jingbohu
Tianchi
Longgang
Erkeshan
Wudalianchi
Yb
Lu
Er
Y
Dy
Tb
Ta
Eu
Th
U
Sm
Nb
Hf
Zr
Nd
Ce
La
Pr
Pb
Rb
Ba
Sr
PC2 (23.4%)
PC1 (59.6%)
B
Contribution (%)
Pr Ce La Nd Zr Sm Hf Rb Sr Ba Nb Eu U Pb Th Ta Lu Yb Dy Er Tb Y
C
Contribution (%)
Er Y Dy Yb Lu Tb Eu Ta Sr Th U Sm Ba Pb Nb Rb La Hf Ce Zr Pr Nd
D
Correlation
Rb Ba Th U Nb Ta La Ce Pb Pr Sr Nd Sm Zr Hf Eu Tb Dy Er Y Yb Lu

Figure 11

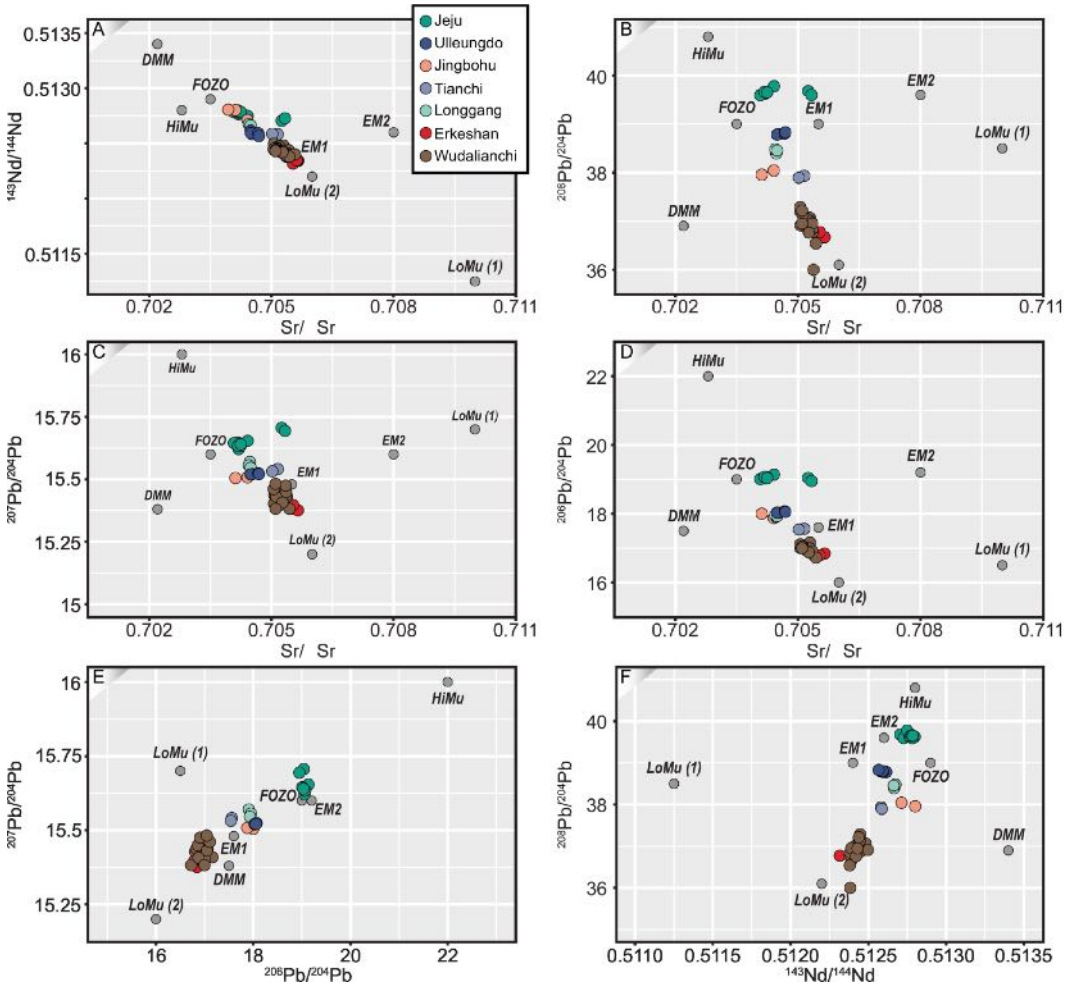
A
B
C
D
E
F
Jeju
Ulleungdo
Jingbohu
Tianchi
Longgang
Erkeshan
Wudalianchi
DMM
FOZO
HiMu
EM2
EM1
LoMu (1)
LoMu (2)
143Nd/144Nd
Sr/ Sr
208Pb/204Pb
207Pb/204Pb
206Pb/204Pb
0.5135
0.5130
0.5115
0.702
0.705
0.708
0.711
40
38
36
16
15.75
15.5
15.25
22
20
18
16
143Nd/144Nd
0.5110
0.5115
0.5120
0.5125
0.5130
0.5135

Figure 12

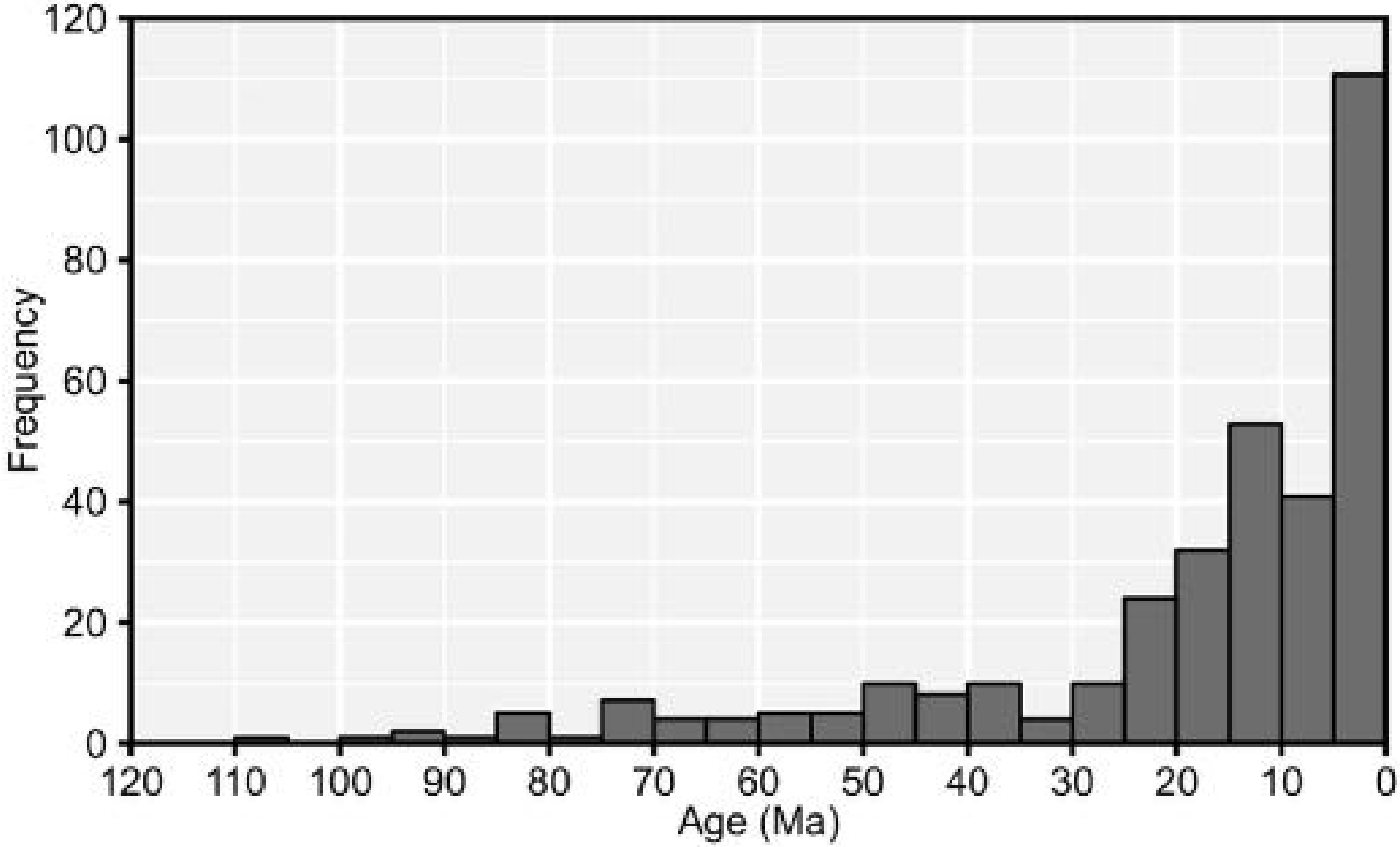
120
100
80
60
40
20
0
Frequency
120
110
100
90
80
70
60
50
40
30
20
10
0
Age (Ma)

Figure 13

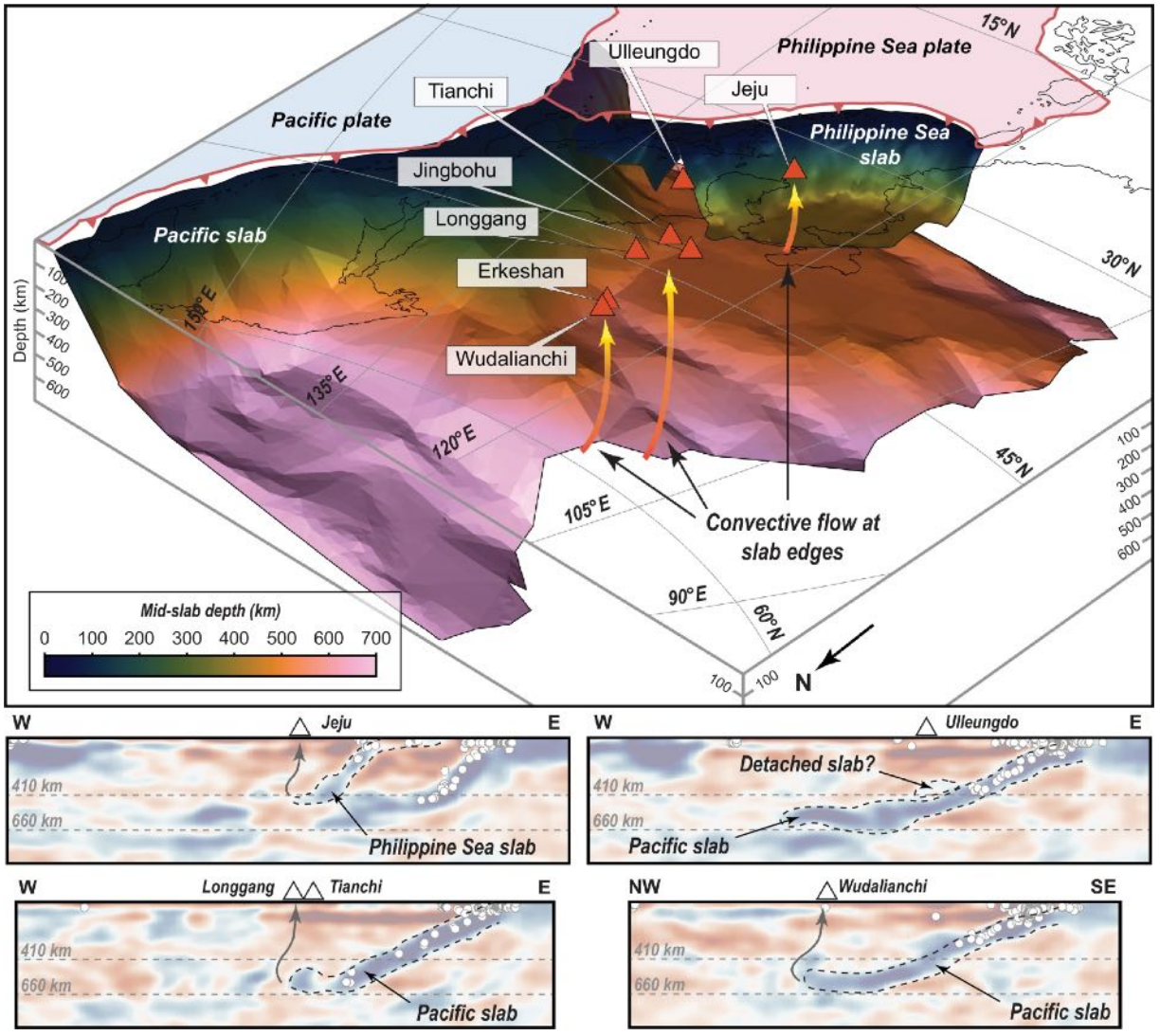
Ulleungdo
Philippine Sea plate
15°N
Tianchi
Jeju
Pacific plate
Philippine Sea slab
Jingbohu
Longgang
Pacific slab
Erkeshan
30°N
Depth (km)
100
200
300
400
500
600
Wudalianchi
135°E
120°E
105°E
45°N
Convective flow at slab edges
90°E
60°N
N
Mid-slab depth (km)
0 100 200 300 400 500 600 700
W
Jeju
E
410 km
660 km
Philippine Sea slab
W
Ulleungdo
E
Detached slab?
410 km
660 km
Pacific slab
W
Longgang
Tianchi
E
410 km
660 km
Pacific slab
NW
Wudalianchi
SE
410 km
660 km
Pacific slab

Figure 14